

Thesis for the Master's
Degree in Chemistry

Atoosa Maleki

Structural and Dynamical
Features in Microscopic and
Macroscopic Hydrogels
Prepared through Chemical
Cross-Linking

60 study points

DEPARTMENT OF CHEMISTRY

Faculty of Mathematics
and Natural Sciences

UNIVERSITY OF OSLO

10/2005



Structural and Dynamical Features in Microscopic
and
Macroscopic Hydrogels Prepared through Chemical
Cross-Linking



Atoosa Maleki

Supervisors



Bo Nyström



Anna-Lena Kjøniksen

DEPARTMENT OF CHEMISTRY

Faculty of Mathematics
and
Natural Sciences

October 2005



University of Oslo

❖ List of Contents

❖ Acknowledgement	6
❖ List of Symbols and Abbreviations.....	8
I. Abstract	12
II. Introduction	14
A. Hydrogels.....	16
B. Microgels	17
C. Cellulose Derivatives	17
D. Hydroxyethylcellulose (HEC).....	19
1. Structure and Preparation	19
2. Applications	21
E. Divinylsulfone (DVS)	22
1. Cross-linking Process	24
F. Gelation.....	25
G. Gel Point	26
III. Experimental Techniques	26
A. Turbidimetry.....	26
B. Rheology.....	28
1. Steady Shear Measurements	29
2. Oscillatory Shear Measurements	31
a) <i>Angular Frequency Dependency of the Complex Viscosity</i>	34
b) <i>Determination of the Gel Point</i>	34
c) <i>Gel Strength Parameter (S)</i>	35

d) <i>Theoretical Models for the Interpretation of n</i>	35
e) <i>Stress Relaxation Experiments</i>	39
C. Small Angle Neutron Scattering (SANS).....	40
D. Light Scattering.....	42
1. Dynamic Light Scattering (DLS)	43
IV. Experimental Section	46
A. Materials and Solution Preparation	46
B. Turbidity Measurements	47
C. Rheology	47
D. Small Angle Neutron Scattering (SANS).....	48
E. Dynamic Light Scattering (DLS).....	49
V. Results and Discussion	49
A. Dilute Solutions.....	50
1. Turbidimetry	50
2. Rheology	51
a) <i>Intrinsic Viscosity and Huggins Coefficient</i>	51
b) <i>Shear Viscosity Measurements</i>	53
3. Dynamic Light Scattering (DLS)	59
a) <i>Correlation Functions</i>	59
b) <i>Fast and Slow Relaxation Times</i>	60
c) <i>Quenching the reaction by HCl</i>	61
(1) <i>q Dependencies of the Fast and Slow Relaxation Modes</i>	63
(2) <i>q Dependency of the Reduced Intensity</i>	65
B. Semidilute Solutions.....	67

1. Turbidimetry	67
2. Rheology	69
a) <i>Steady Shear Measurements</i>	69
b) <i>Oscillatory Shear Measurements</i>	73
(1) Angular Frequency Dependency of the Complex Viscosity	74
(2) Testing of Cox-Merz Rule	76
(3) Determination of the Gel Point	77
(4) Gel Strength Parameter (S) and the Relaxation Exponent (n)	82
(5) Zero-Shear Viscosity	84
c) <i>Stress Relaxation Experiments</i>	85
3. Small Angle Neutron Scattering (SANS)	87
4. Dynamic Light Scattering (DLS)	90
VI. Conclusions	95
VII. Appendix	97
VIII. References	98



❖ Acknowledgement

My principle debt of thanks is to my supervisors professor Bo Nyström and Anna-Lena Kjoniksen for their insightful remarks, inspirational suggestions, helpful advices and supportive guidance. Having the honor of attending in three conferences (Wadahl 2003, Wadahl 2004, France 2005) as their student, has given me the pleasure of getting benefit of their immense knowledge more.

My expression of appreciation is to Kenneth Knudsen for his support at IFE to do the SANS measurements.

I would like to thank the Polymer group at University of Oslo for their friendly cooperation. I wish to express my deepest gratitude to Huaitian Bu for her extremely cordial assistance.

My gratitude to all faithful friends out of the university and colleagues at job that helped me a lot in the procedure of doing this thesis.

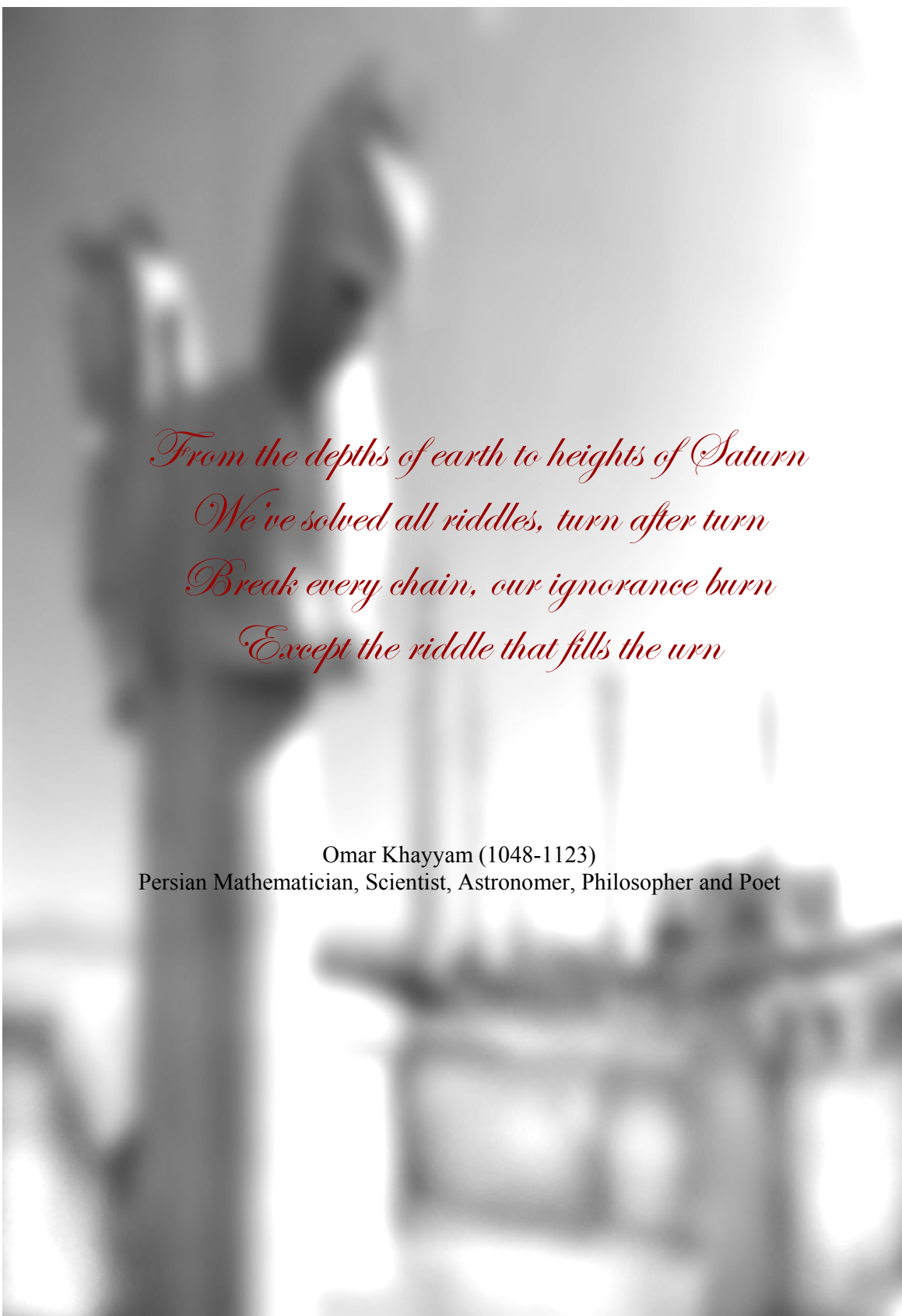
I owe a debt of gratitude to my dear uncle Morteza Lavasani, whose emotional and financial support were instrumental in making this paper a reality.

A special thank to my dear parents and beloved sisters, for their everlasting support, great affection and their pure love.

Above all else, thank God for creating and making me what I am. May his merciful and supportive grace be upon the all forever and me.

Atoosa Maleki

October 2005



*From the depths of earth to heights of Saturn
We've solved all riddles, turn after turn
Break every chain, our ignorance burn
Except the riddle that fills the urn*

Omar Khayyam (1048-1123)
Persian Mathematician, Scientist, Astronomer, Philosopher and Poet

❖ List of Symbols and Abbreviations

A_2	Second Virial Coefficient
A_f	Amplitude of the Fast Mode
A_s	Amplitude of the Slow Mode
a	A Coefficient ($ \eta^*(\omega) = aS\omega^m$)
B	Empirical Factor
c_p	Polymer Concentration
C^*	Overlap Concentration
Cell.....	Cellulose
Conc.	Concentration
CP.....	Cloud Point
D	Diffusion Coefficient
D_c	Cooperative Diffusion Coefficient
D_m	Mutual Diffusion Coefficient
DLS.....	Dynamic Light Scattering
DS.....	Degree of Substitution
DVS.....	Divinylsulfone
d	Space Dimension
d_f	Fractal Dimension
EO.....	Ethylene Oxide Group
f	Applied Frequency (s^{-1})
$G(i)$	Initial Relaxation Modulus

$G(t)$	Relaxation Modulus
$G'(\omega)$	Storage Modulus (or G')
$G''(\omega)$	Loss Modulus (or G'')
GP	Gel Point
$g^1(q,t)$	First Order Electric Field Correlation Function
$g^2(q,t)$	Measured Homodyne Intensity Autocorrelation Function
HEC.....	Hydroxyethylcellulose
$I(q)$	Scattering Intensity
I_t	Transmitted Light Intensity
I_o	Incident Light Intensity
k'	Huggins Coefficient
k_B	Boltzmann's Constant
L	Characteristic Length
l	Light Path Length in the Cell (in Turbidimetry)
M	Mass of a Molecular Cluster
M_n	Number Average Molecular Weight
M_w	Weight Average Molecular Weight
MS.....	Molar Substitution
m	Complex Viscosity Relaxation Exponent ($\eta^* \sim \omega^m$)
N_A	Avogadro's Constant ($6.022 \times 10^{23} \text{ mol}^{-1}$)
n	Relaxation Exponent
n'	Power Law Parameter ($G' \sim \omega^{n'}$)
n''	Power Law Parameter ($G'' \sim \omega^{n''}$)

n_{coup}	Coupling Parameter
n_{ref}	Refractive Index
P	Bond Probability (A Measure of Connectivity)
P_c	Critical Extent of Reaction
q.....	Wave Vector
R_g	Radius of Gyration
R_h	Hydrodynamic Radius
Ref.	Reference
r	Scaling Exponent
S	Gel Strength Parameter
SANS	Small Angle Neutron Scattering
T	Temperature
t.....	Time
$\tan \delta$	Damping factor or Loss Tangent
z.....	Power Law Exponent ($I(q) \sim q^z$)
α	Power Law Index ($\eta \propto \dot{\gamma}^{(\alpha-1)}$)
α_f	Power Law Exponent ($\tau_f^{-1} \propto q^{\alpha_f}$)
α_s	Power Law Exponent ($\tau_s^{-1} \propto q^{\alpha_s}$)
β	Stretch Exponent
Γ	Gamma Function
γ	Strain
γ_0	Maximum Amplitude for the Strain
$\dot{\gamma}$	Shear Rate

δ	Phase Angle
ε	Relative Distance from the Gel Point
η	Viscosity
η_{red}	Reduced Viscosity
η_{sp}	Specific Viscosity
η_z	Zero - Shear Viscosity
η_o	Viscosity of Solvent
$[\eta]$	Intrinsic Viscosity
$ \eta^* $	Absolute Value of Complex Viscosity
θ	Scattering Angle
λ	Wavelength
ξ	Screening Length
ξ_h	Hydrodynamic Correlation Length
ρ	Separating Parameter
$d\Sigma/d\Omega$	Coherent Macroscopic Scattering Cross Section
σ	Stress
σ_o	Maximum Amplitude for the Stress
τ	Turbidity
τ_f	Fast Relaxation Time
τ_s	Slow Relaxation Time
τ_{se}	Slow Effective Relaxation Time
ϕ	Power Law Exponent ($\eta \sim t^\phi$)
ω	Angular Frequency (rad/s)

I. Abstract

Rheological, dynamical, turbidity, and structural features during the cross-linking process of dilute and semidilute hydroxyethylcellulose (HEC) solutions in the presence of the cross-linker agent divinylsulfone (DVS) have been investigated at different polymer and cross-linker concentrations. For the *semidilute* system, a *macroscopic gel* evolves in the course of time if the cross-linker addition is sufficiently high, and the gelation time decreases as the cross-linker concentration or polymer concentration increases, while for the *dilute* polymer solution, only small non-connected aggregates, *microgels*, are formed. For dilute solutions under shear flow, intramolecular interactions dominate initially, followed by intermolecular associations and the formation of aggregates at longer times. Depending on the shear rate, the aggregates continue to grow until they reach a certain size where an incipient breakup of interaggregate chains can be observed. The delicate interplay between intramolecular and intermolecular association effects is governed by factors such as the magnitude of the shear rate, polymer concentration, and cross-linker density. At quiescent state, dynamic light scattering detected only interchain aggregation of HEC during the cross-linker reaction, and the magnitude and start of this effect depend on the cross-linker concentration. The growth of clusters has been investigated at various stages in the course of the cross-linking process by quenching the reaction mixture to a lower pH. The rheological results favor the percolation model for the semidilute sample at the gel point. The slow relaxation time determined from dynamic light scattering experiments increases and the sample becomes more heterogeneous in the course of gelation. In the post-gel region, the gels shrink during a long time and this

phenomenon is accompanied by a strong turbidity enhancement. Small angle neutron scattering results from samples quenched to a certain stage in the post-gel regime, disclose growth of the heterogeneity in the gel with increasing level of cross-linker addition. At smaller length scales, no effect of cross-linker addition could be detected on the structural organization, and the wave vector dependence of the scattered intensity in this domain suggests that the HEC chains are locally stretched.

Persian abstract:

خلاصه

خواص پویائی¹، رئولوژیکی²، ساختاری و کدري³ محلول رقیق و نیمه غلیظ⁴ هیدروکسی اتیل سلولز (HEC)⁵، تحت فرآیند اتصالات عرضی⁶ با غلظتهای متفاوت پلیمر و اتصال دهنده⁷ بررسی شده است. عامل اتصال دهنده اضافه شده به محلولها، دی وینیل سولفون (DVS)⁸ می باشد. پیدایش تدریجی ماکروژل⁹ در سیستم نیمه غلیظ در حضور میزان کافی اتصال دهنده، قابل مشاهده می باشد و زمان تشکیل ژل با افزایش غلظت پلیمر و اتصال دهنده کاهش می یابد، در حالیکه در سیستم رقیق، تنها توده های کوچک اتصال نیافته، (اتصالات درون مولکولی)¹⁰ میکروژل¹¹، تشکیل می شوند. در مراحل اولیه جریان برشی¹² اعمال شده برای سیستم رقیق، فعل و انفعالات درون مولکولی غالب است و با گذشت زمان و افزایش جریان برشی، پیوستگی بین مولکولی¹³ و پیدایش توده های بهم پیوسته قابل مشاهده می باشد. پیدایش این تجمعات تا مرحله زمانی مشخصی ادامه می یابد، که در آن زمان تفکیک بین زنجیره ای در سیستم اتفاق می افتد و این امر تابع شدت برشی¹⁴ می باشد. نبرد حساس بین تجمعات بین مولکولی و درون مولکولی در محلولها، وابستگی زیاد به شدت برش، غلظت پلیمر و غلظت اتصال دهنده دارد. ساختار محلولها با تکنیک تفرق نور پویا (DLS)¹⁵ بررسی شده است و نتایج بدست آمده فقط تجمعات بین مولکولی را برای محلول هیدروکسی اتیل سلولز در حضور اتصال دهنده تحت فرایند ژل شدن نشان می دهد، که میزان و زمان شروع آن بستگی به غلظت اتصال دهنده دارد. رشد توده ها در مراحل مختلف فرایند اتصالات عرضی توسط متوقف کردن واکنش با کاهش خاصیت اسیدی (pH)

¹ Dynamic

² Rheological

³ Turbidity

⁴ Semidilute

⁵ Hydroxyethylcellulose (HEC)

⁶ Cross-Linking

⁷ Cross-Linker

⁸ Divinylsulfone (DVS)

⁹ Macrogel

¹⁰ Intramolecular

¹¹ Microgel

¹² Shear Flow

¹³ Intermolecular

¹⁴ Shear Rate

¹⁵ Dynamic Light Scattering

قابل بررسی است. نتایج رئولوژیکی، مدل پرکوله¹⁶ را برای سیستم نیمه غلیظ در نقطه ژل تأیید می کند. زمان آسایش مولکولی کند¹⁷ که توسط تکنیک تفرق نور پویا (DLS) تعیین شده، تحت فرایند ژل شدن افزایش می یابد و رشد ناهمگنی¹⁸ سیستم قابل نتیجه گیری است. در مراحل فرا ژل¹⁹، در بلند مدت، ژل جمع و کوچک²⁰ می شود و این پدیده همراه با افزایش کداری محلول می باشد. برای نمونه هایی که واکنش اتصالات عرضی در مرحله فرا ژل، توسط اضافه کردن اسید و کاهش خاصیت اسیدی (pH) در آنها متوقف شده، تکنیک تفرق کم زاویه نوترونی (SANS)²¹ انجام شده است. نتایج بدست آمده رشد ناهمگنی در ژل با افزایش میزان اتصال دهنده را تأیید می کند. در مقیاس طولی کوچکتر (بردار موجی²² بزرگ) اثر افزایش اتصال دهنده بر ساختار سیستم نمایان نمی باشد، و وابستگی بردار موجی (q) نسبت به شدت تفرق در این ناحیه نشان می دهد که زنجیره های HEC به صورت موضعی²³ ارتجاع می یابند.

¹⁶ Percolation Model

¹⁷ Slow Relaxation Time

¹⁸ Heterogeneous

¹⁹ Post-gel Regime

²⁰ Shrink

²¹ Small Angle Neutron Scattering (SANS)

²² Wave Vector

²³ Locally

II. Introduction

A. Hydrogels

Hydrogels are three-dimensional networks made of cross-linked hydrophilic or amphiphilic polymers. Cross-links can result from physical^{1,2} or chemical bonding.^{3,4} Hydrogels (the polymer concentration is usually low (typically 1 wt %)) are materials which, when placed in excess water, are able to swell and retain large volume of water in its swollen three-dimensional structure without dissolution. This particular behavior makes them very attractive for many biomedical applications including contact lenses⁵, time controlled drug delivery systems⁶, but also for ion exchange⁷, and separating membrane⁸ superabsorbents. The hydrophilicity is due to the presence of water-solubilizing groups, such as $-OH$, $-COOH$, $-CONH_2$, $-CONH-$, $-SO_3H$, etc. The stability of the structure is due to the presence of a three-dimensional network. The swollen state results from a balance between the dispersing forces acting on hydrated chains and cohesive forces that do not prevent the penetration of water into the network. Cohesive forces are most often due to covalent cross-linking. Physical interactions are electrostatic, hydrophobic, or dipole-dipole in character. The degree and nature of cross-linking and the tacticity and crystallinity of the polymer are responsible for its characteristics in the swollen state⁹. The ability to imbibe water and ions without the loss of shape or mechanical strength is valuable in many natural hydrogels, such as those found in muscle, tendons, cartilage, intestines, and blood.

B. Microgels

The gelation of a semidilute polymer solution results from the formation of a connected network via intermolecular cross-links that can be established by various mechanisms, such as attractive interactions between hydrophobic groups^{10,11}, temperature-induced attraction between polymer chains¹²⁻¹⁴, and cross-links mediated by a chemical cross-linking agent.^{3,15,16} However, if a dilute polymer solution is, e.g., chemically cross-linked, the connectivity is lost and non-linked aggregates of finite size are formed, which may be referred to as microgels.¹⁷

Microgels are cross-linked colloidal particles that can swell by the absorption of many times their weight of solvent and exhibit a behavior ranging from that of polymer solutions to that of hard spheres.^{18,19} From an application point of view, the microgel particles can respond to the environmental change much faster than bulk gels due to much smaller size of the particles. Unusual properties of microgels lead to various applications including the automotive surface coatings, and controlled drug delivery.¹⁸ Many methods have been developed for preparing microgels, including emulsion polymerization, inverse microemulsion polymerization, anionic copolymerization, and cross-linking of neighboring polymer chains.¹⁸

C. Cellulose Derivatives

Cellulose is an $\beta-1 \rightarrow 4-D$ -anhydroglucopyranose copolymer that serves as the major structural component of plants (*Figure 1*). When the cellulose molecule is extended, it is a flat ribbon with hydroxyl groups protruding laterally and capable

of forming both intra- and intermolecular hydrogen bonds. This form allows the strong interaction with neighboring chains that makes dissolution difficult. In fact, strongly interactive solvents are necessary for solubilization. Molecular weights range from 5×10^5 to 1.5×10^6 , depending on the source.²⁰

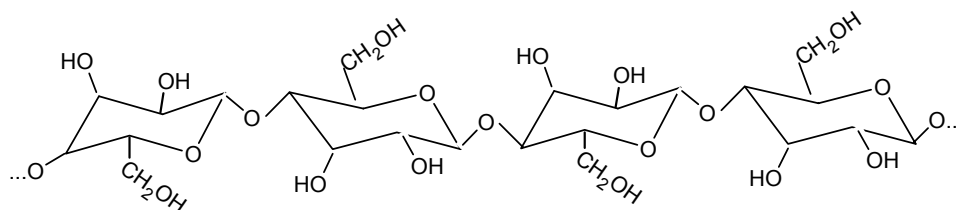


Figure 1. The chemical structure of cellulose.

The anhydroglucose moiety contains three reactive hydroxyl functions: one primary at the C-6 position, and two secondary at the C-2 and C-3 positions. These hydroxyl functions provide the sites for alkylation to yield cellulose ether derivatives.

The abundance of hydroxyl groups leads to the formation of an intricate array of intramolecular and intermolecular hydrogen bonds during biosyntheses. Intramolecular hydrogen bonding between adjacent anhydroglucose rings enhances the linear integrity of the polymer chain. Such intramolecular hydrogen bonding not only affects chain rigidity, but also the reactivity of the hydroxyl functions, particularly of the C-3 hydroxyl groups which hydrogen bond strongly to the ring oxygen atoms on adjacent anhydroglucose units.

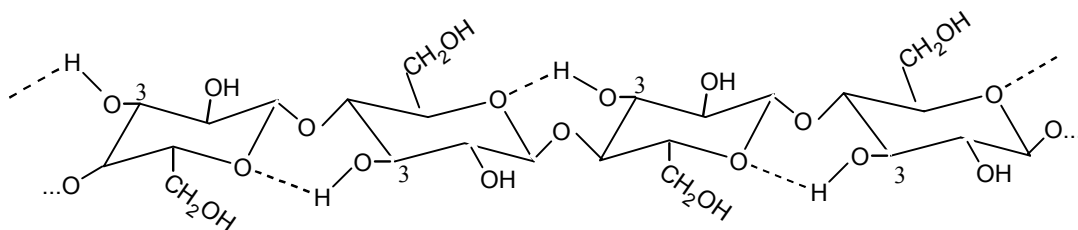


Figure 2. Conformational structure representation of cellulose depicting intramolecular hydrogen bonding between OH at C-3 and ring oxygen.

The regular rod-like cellulose chains allow an efficient close-packing arrangement, permitting intermolecular hydrogen bonding to yield a fibrillar tertiary structure of high order. Several methods have been reported for determining the ordered fraction of cellulose. The high degree of order and cohesive energy among chains is responsible for cellulose being insoluble in most solvents, including water, and is the main obstacle to overcome in synthesizing soluble derivatives, so it is necessary to make modifications to improve its solubility in aqueous media. This is accomplished by making cellulose derivatives, which are more hydrophilic in nature.²¹ In the present study the hydrophilic hydroxyethylcellulose (HEC) is employed.

D. Hydroxyethylcellulose (HEC)

1. Structure and Preparation

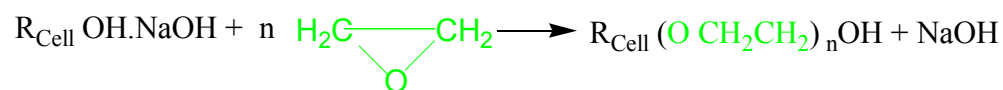
HEC is a hydrophilic non-ionic polymer, typically prepared by the reaction of cellulose with ethylene oxide.



Figure 3. HEC is white or yellowish powder.

Hydroxyethylcellulose (HEC) is prepared by nucleophilic ring opening of ethylene oxide, by the hydroxyl anions on the anhydroglucose ring of cellulose. HEC has a little surface activity in solution and is compatible with a wide range of surfactants and salts. To quantify the substitution of ethylene oxide (EO) groups along the cellulose backbone, the notations DS and MS have been introduced. The degree of substitution (DS) denotes the number of hydroxyl groups that have been substituted on each anhydroglucose unit, and can thus vary between 0 and 3. Due to the ability of ethylene oxide to form short oligo (ethylene oxide) chains, the molar substitution (MS) is employed. MS is equal to the total number of ethylene oxide groups per anhydroglucose unit.²² *Figure 4* shows a schematic representation of preparation and structure of HEC.

(a)



(b)

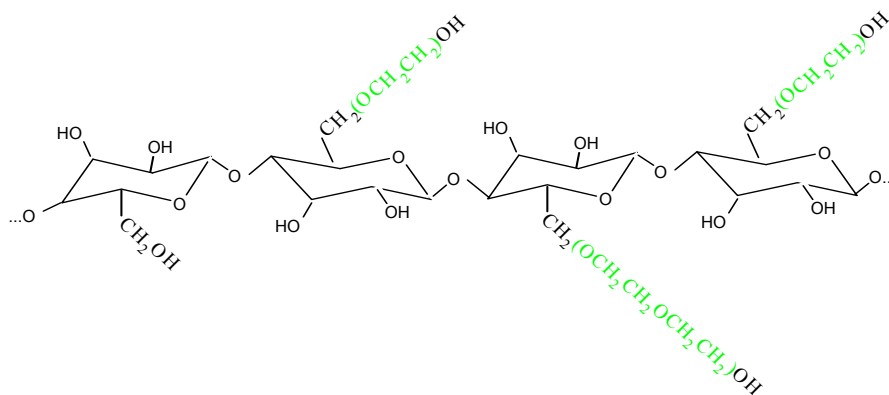


Figure 4. (a) HEC is formed by the reaction of alkali cellulose with ethylene-oxide; (b) schematic representation of the chemical structure of HEC.

2. Applications

Because of its broad compatibilities, HEC is widely used in applications and products that require thickening, water binding, lubricating, film forming, and protective colloid or stabilizing properties (See *Table 1*).^{20,21}

Table 1. Uses of Hydroxyethylcellulose²¹.

Property	Applications
Protective colloid	Vinyl acetate and vinyl chloride polymerization
	Pharmaceutical emulsions
	Latex paints
Lubricity	Wallpaper adhesives
	Pharmaceutical gels
	Welding rods
Water binding	Plastics
	Cements, also as set retarder
	Texture paints
	Foundry cores
	Ceramic glaze
	Welding rods
	Printing pastes
Film forming	Size-press solutions
	Fabric finishes
	Aerosol starches
Thickener	Glass-fiber size
	Adhesives
	Latex paints
	Shampoos and hair dressings
	Toothpaste
	Cosmetic creams and lotions
	Printing pastes and inks
Completion and work-over fluids	
Joint cements	

E. Divinylsulfone (DVS)

The agent divinylsulfone (DVS) has been widely used to cross-link hydroxyl containing polymers to prepare gels, microgels, and nanoparticle networks in alkaline solutions (around pH = 12 or higher). The chemical structure of DVS is given in *Figure 5a* and the function of the cross-linker is indicated in *Figure 5b*. This reaction

is an example of Michael addition chemistry, so in principle no byproducts should be generated. However, in practice DVS is hydrolyzed by water (slowly at neutral pH and more rapidly in alkaline solution; see *Figure 5c*).²³

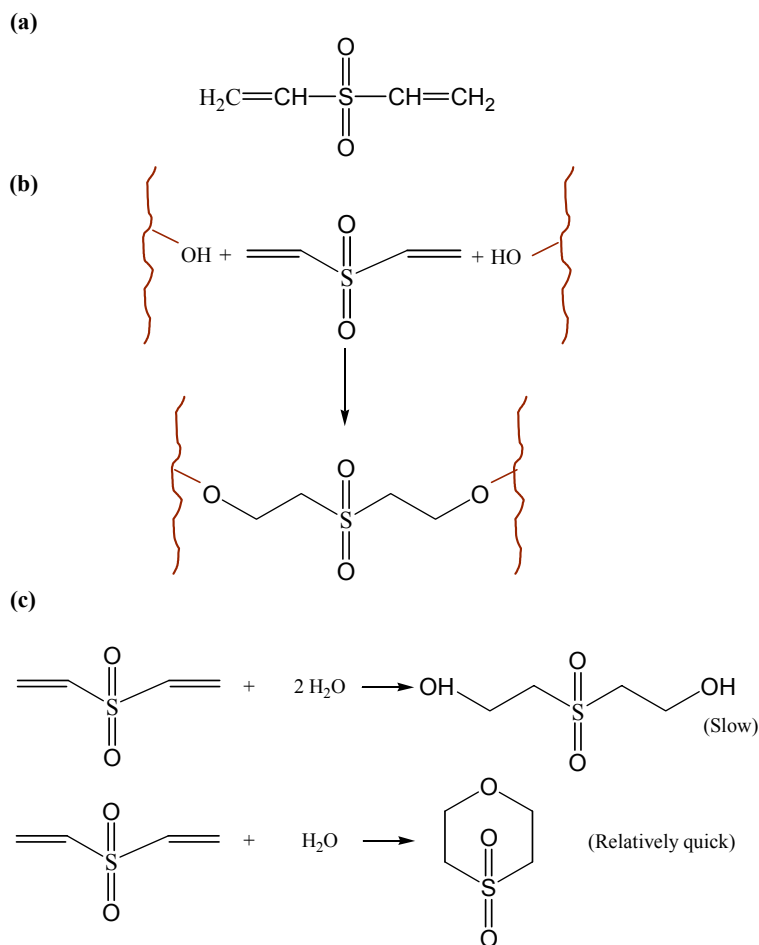


Figure 5. (a) The chemical structure of DVS; (b) Reaction scheme for cross-linking of the hydroxyl-functional polymers with DVS; (c) Side reaction of DVS in aqueous solution at neutral and alkaline pH.

One advantage of using DVS as a cross-linker is that, in principle, the extent of incorporation of the DVS can be assessed by sulfur microanalyses.²³

1. Cross-linking Process

There are two types of cross-linking processes, that is, *inter-* and *intrapolymer* cross-linking. The former allows the increase of the molecular weight (M_w) of a cross-linked polymer via the coupling of two or more polymer chains. The latter does not alter M_w but affects the quantities relating to a polymer chain dimension, e.g., hydrodynamic radius (R_h) as well as radius of gyration (R_g), because the cross-linking should take place within the same polymer chain.²⁴

A proposed scheme for the cross-linker reaction and the formation of a cross-linked network for dilute and semidilute HEC solutions in the presence of DVS are illustrated in *Figure 6* and *Figure 7*, respectively.

Dilute system

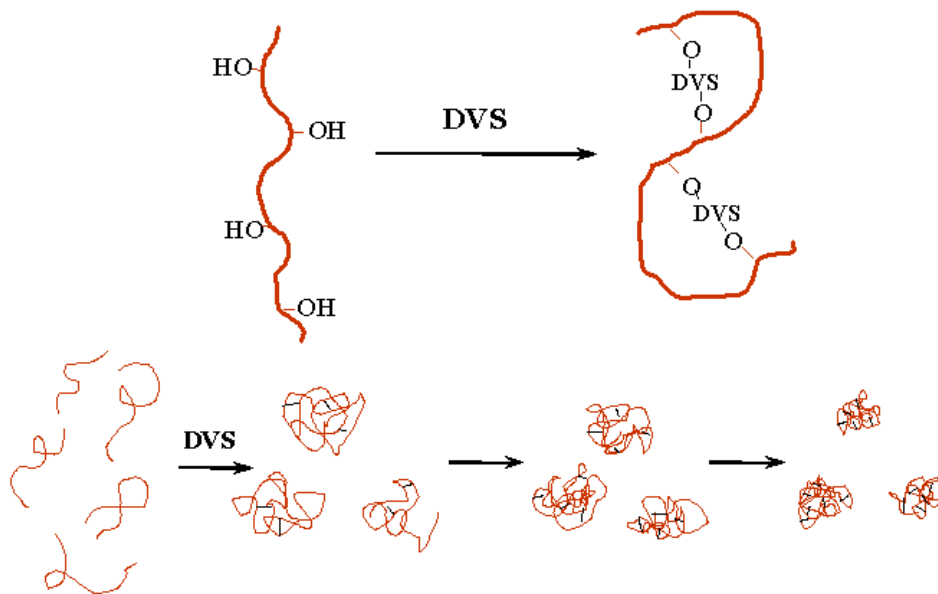


Figure 6. An illustration of cross-linking reaction for a *dilute* HEC solution, in the presence of DVS as a cross-linker.

Semi-dilute system

The mechanism is the same as in *Figure 5b* but in this case a connected network is formed.

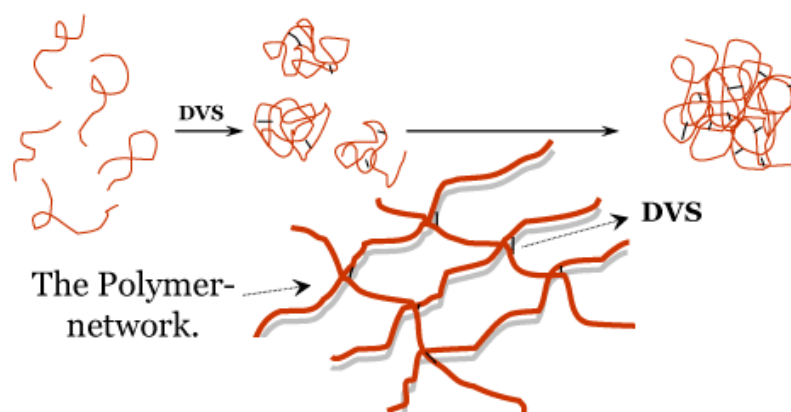


Figure 7. An illustration of cross-linking reaction for a semidilute HEC solution, in the presence of DVS as a cross-linker

F. Gelation

The problem of the transition of polymer solutions into gels (gelation) has always been considered as a classical subject of colloid chemistry.²⁵ Gelation of a polymer solution can be characterized as a process involving a continuous increase in viscosity accompanied by a gradual enhancement of elastic properties. Gelation results in ‘freezing’ of the whole system into a uniform non-flowing elastic mass, which is a gel resulting from the formation of a polymer structural network, encompasses the whole bulk of the system, and retains the solvent. The main cause of gelation in polymer systems is the enhancement of interactions between the dissolved polymer macromolecules or their aggregates. Gelation is usually related to poorer thermodynamic conditions and phase separation.^{26,27} In this work, gelation occurs

through a chemical reaction with the aid of a chemical cross-linker agent. In this investigation, two different types of gels have been studied, namely microgels, which are made by the intramolecular associations in dilute polymer solutions, and macroscopic gels, which are prepared by the intermolecular associations in semidilute polymer solutions. The word ‘gel’ refers to ‘macroscopic gel’ in this thesis.

G. Gel Point

A polymer at its gel point (GP), the critical gel, is in a transition state between liquid and solid. Its molecular-weight distribution is infinitely broad ($M_w / M_n \rightarrow \infty$) and molecules range from the smallest un-reacted monomer to the infinite cluster. The molecular motions are correlated over large distances but the critical gel has no intrinsic size scale. The polymer reaches the GP at a critical extent of reaction ($p \rightarrow p_c$). The liquid polymer before the GP ($P < P_c$) is called a sol because it is soluble in good solvents. The solid polymer beyond the GP ($P_c < P$) is called a gel, which is not soluble, even in a good solvent (only valid for chemically cross-linked gels). However, low molecular weight molecules (sol fraction) are still extractable.²⁸

III. Experimental Techniques

A. Turbidimetry

Turbidity is a measure of how opaque the sample is, and this technique is a powerful method to characterize the thermodynamic and associative properties of

polymer solutions. To measure the turbidity, a spectrophotometer is used. In this instrument, a light source illuminates the sample with light of a certain wavelength and the intensity of the transmitted light (I_t) is registered.



Figure 8. The spectrophotometer

The spectrophotometer that has been used for this system is a computer-controlled *Thermo Spectronic Helios Gamma* with a good temperature control in the range (0-100 °C). It is a single beam UV-Vis spectrophotometer with a wavelength range 190 -1100 nm and a fixed 2 nm bandwidth.

It can measure in two modes:

- Absorbance (how much light is absorbed by the sample)
- Transmittance (the percentage of the incoming light that goes through the sample)

The transmittance was measured in this study.

To calculate the turbidity from the measured transmittance, the following equation is used ⁴:

$$\tau = \left(-\frac{1}{l}\right) \ln\left(\frac{I_t}{I_0}\right)$$

$$\tau = \left(-\frac{1}{1_{cm}}\right) \ln\left(\frac{I_t}{100}\right)$$

(1)

B. Rheology

Rheology is the science of the deformation and flow of matter. It is concerned with the response of materials to mechanical force. That response may be irreversible flow, reversible elastic deformation, or a combination of both. Deformation is the relative displacement of points of a body. It can be divided into two types: flow and elasticity. Flow is an irreversible deformation; when the stress is removed, the material does not revert to its original configuration. This means that work is converted into heat. Elasticity is almost a reversible deformation; the deformed body recovers its original shape, and the applied work is largely recoverable. Viscoelastic materials show both flow and elasticity features.²⁹

The *Paar-Physica MCR 300* rheometer, utilized in this study, is a very accurate instrument to monitor various rheological quantities. It is equipped with a Peltier plate temperature unit that gives a very good temperature control (± 0.05) over an extended

time. A cone-and-plate geometry, with a cone angle of 1° and a diameter of 75 mm has been used in this study (See *Figure 9*).

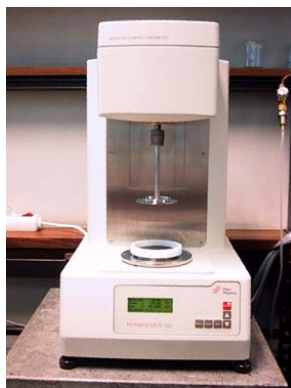


Figure 9. The Rheometer

1. Steady Shear Measurements

In steady shear measurements, the cone will rotate, and each point is measured at a different shear rate, giving us the shear rate ($\dot{\gamma}$) dependency. In this mode, the viscosity of the sample can be determined. For some systems the viscosity is shear rate independent; giving a viscosity (η) that does not vary with the shear rate. These systems are called Newtonian systems. Some polymer systems will exhibit a shear-thinning behavior (the viscosity decreases with increasing shear rate). This behavior can often be attributed to intermolecular associations and/or entanglements that are disrupted by the shear forces. A shear-induced viscosity drop can also be observed in dilute solution through alignment of the polymer chains in the shear field. In addition, some systems exhibit shear thickening at low shear rates, and shear-thinning at higher shear rates. Stretching and alignment of the polymer chains, giving rise to easier

access for intermolecular associations, usually cause shear-thickening. At high shear rates, the associations breakup and the system exhibits shear thinning behavior.³⁰ At low shear rates, the viscosity assumes a constant value, which yields the zero-shear viscosity. The shear rate dependency of the viscosity can be represented by eq. 2:

$$\eta \propto \dot{\gamma}^{(\alpha-1)}$$

↓
Power law index

↘

→

↙

$\alpha < 1$ Shear thinning system

$\alpha = 1$ Newtonian system

$\alpha > 1$ Shear thickening system

(2)

The intrinsic viscosity, $[\eta]$, and Huggins coefficient, k' , can be determined from a measurement series in dilute polymer solutions.

The specific viscosity, η_{sp} , is given by:

$$\eta_{sp} = \frac{\eta_z - \eta_0}{\eta_0} \quad (3)$$

where η_z is the zero-shear viscosity of the polymer solution, and η_0 is the viscosity of the solvent.

The reduced viscosity, η_{red} , is given by:

$$\eta_{red} = \frac{\eta_{sp}}{c_P} \quad (4)$$

where c_P is the polymer concentration.

The intrinsic viscosity is given by:

$$[\eta] = \lim_{c \rightarrow 0} \frac{\eta_{sp}}{c_P} \quad (5)$$

The intrinsic viscosity and Huggins coefficient (k') can be determined from eq. 6.

$$\frac{\eta_{sp}}{c_P} = [\eta] + k' \cdot [\eta]^2 \cdot c_P \quad (6)$$

2. Oscillatory Shear Measurements

In oscillatory shear measurements, the cone or plate may oscillate and each point is measured at a different angular frequency (ω).

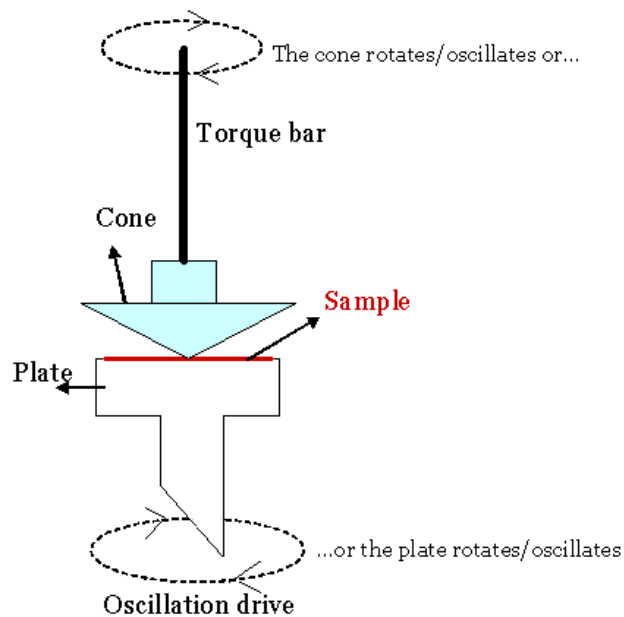


Figure 10. A schematic picture of the rheometer.

In order to determine the dynamic properties of the system, oscillatory shear measurements are conducted. When a sample is constrained in a cone and plate assembly, an oscillating strain at a given frequency can be applied to the sample. After an initial start-up period, a stress develops in direct response to the applied strain due to transient sample and instrumental responses. If the strain has an oscillating value with time, the stress must also be oscillating in time. These two waveforms can be represented as in the following way:

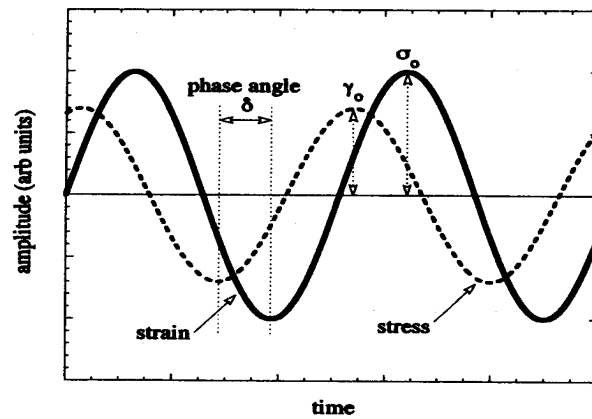


Figure 11. An illustration of oscillating strain and stress response.

When a tangential displacement is applied to the lower plate, a strain in the sample is produced. That displacement is transmitted directly through the sample. The upper cone will react in proportion to the applied strain to give a stress response. If the viscoelastic material is in the instrument, some energy is stored and some dissipated, the stored contribution will be in phase whilst the dissipated or loss contribution will be out of phase with the applied strain³¹. The stress and strain can be written as:

$$\gamma = \gamma_0 \sin \omega t \quad (7)$$

$$\sigma = \sigma_0 \sin(\omega t + \delta) = \sigma_0 \cos \delta \sin \omega t + \sigma_0 \sin \delta \cos \omega t \quad (8)$$

where t is the time and γ_0 and σ_0 are the maximum amplitudes for the strain and stress, respectively.

The stress can also be expressed as:

$$\sigma = \gamma_0 [G'(\omega) \sin \omega t + G''(\omega) \cos \omega t] \quad (9)$$

where $G'(\omega)$ is the storage modulus (elastic response) and $G''(\omega)$ is the loss modulus (viscose response). G' and G'' vary with the phase angle as:

$$\tan \delta = \frac{G''}{G'} \quad (10)$$

δ is the phase difference in radians between the peak value of the stress, and the peak value of the strain, which is constant with time at any given frequency.³

The absolute value of the complex viscosity can be determined from⁴:

$$|\eta^*| = \frac{\sqrt{G'^2 + G''^2}}{\omega} \quad (11)$$

ω is the angular frequency, which is equal to $2\pi f$ where f is the applied frequency measured in Hertz.

a) Angular Frequency Dependency of the Complex Viscosity

The angular frequency dependency of the complex viscosity gives information about the solid-like or liquid-like behavior of the system, and can be expressed in terms of a power law ⁴:

$$|\eta^*| \propto \omega^m \begin{cases} m = 0 & \text{Liquid-like behavior} \\ -1 < m < 0 & \text{Viscoelastic behavior} \\ m = -1 & \text{Solid-like behavior} \end{cases} \quad (12)$$

b) Determination of the Gel Point

The gel point can be determined by oscillatory shear measurements. According to the model of Chambon and Winter^{32,33}, the gel point is characterized by a frequency independency of $\tan \delta$, and the following power-law of G' and G'' is valid:

$$G'(\omega) \propto G''(\omega) \propto \omega^n \quad (13)$$

where n ($0 < n < 1$) is the relaxation exponent.

The gel point can be determined by plotting $\tan \delta$ at several frequencies against the gel forming parameter (e.g., time and temperature), and determining the point where $\tan \delta$ is frequency independent. The gel point can be also determined by finding the point where the slopes of G' and G'' versus ω are the same in a log-log plot.³

$$G' \propto \omega^{n'}, G'' \propto \omega^{n''} \quad (14)$$

At the gel point: $n' = n'' = n$

c) Gel Strength Parameter (S)

To characterize how stiff a sample is at the gel point, the gel strength parameter (S) is determined, which is dependent on the cross-linking density and the molecular chain flexibility.³³ The values of n and S for an incipient gel can be determined from a power law describing the frequency dependency of the absolute value of the complex viscosity.³⁴

$$|\eta^*(\omega)| = aS\omega^m \quad (15)$$

$$m = n-1 \quad (16)$$

$$a = \frac{\pi}{\Gamma(n)\sin(n\pi)} \quad (17)$$

where $\Gamma(n)$ is the gamma function and m is the complex viscosity relaxation exponent and is directly related to the relaxation exponent n.

d) Theoretical Models for the Interpretation of n

A number of theoretical models³⁵⁻⁴³ have been developed to predict the value of the relaxation exponent. The present understanding of the phenomenology of

gelation is essentially based on concepts such as dynamic scaling, fractal analysis, and percolation of clusters. The growing clusters, which appear as the connectivity increases near the gelation threshold, may be described in terms of the fractal geometry on the length scales between the monomer size and the correlation length of the connectivity.

The structure of the incipient gel can be described by a fractal dimension, d_f , which is defined by:

$$R_g^{d_f} \propto M \quad (18)$$

where R_g is the radius of gyration and M is the mass of a molecular cluster. A dynamical scaling analysis of flexible fractals in the Rouse limit (no hydrodynamic interaction), taking into account the effect of screening of excluded-volume and hydrodynamic interactions but ignoring entanglement effects, yield for a monodisperse solution of polymers of fractal dimension d_f a viscoelastic exponent of^{3,37,38}:

$$n = \frac{d_f}{2 + d_f} \quad (19)$$

If we assume that the fractal dimension is located in the range $1 \leq d_f \leq 3$, then eq. 19 predicts that the relaxation exponent is restricted for $1/3 \leq n \leq 3/5$. When polydisperse clusters near the gelation threshold are considered and Rouse dynamics prevails, the relationship for non-entangled systems can be described as:

$$n = \frac{d_f(r-1)}{(d_f+2)} \quad (20)$$

where r is a scaling exponent describing the cluster size distribution function near the gel point:

$$r = 1 + \frac{d}{d_f} \quad (21)$$

where d ($d = 3$) is the space dimension. From percolation statistics ($d_f = 2.5$ & $r \approx 2.2$), it follows that $n = 2/3$. On the other hand, based upon a suggested^{37,38} isomorphism between the complex modulus and the electrical conductivity of a percolation network with randomly distributed resistors and capacitors, a value of $n = 0.72$ has been predicted. Since these values are close to each other, dynamic rheological experiments do not allow distinguishing between these predictions. In a number of oscillatory shear studies on incipient gels of various natures, values of n in the whole range $0 < n < 1$ have been reported⁴⁴. To rationalize these values, Muthukumar developed a theoretical model⁴¹ in which it is assumed that variations in the strand length between cross-linking points of the incipient gel network give rise to changes of the excluded volume interactions. It is anticipated that increasing strand length should enhance the excluded volume effect. To account for this effect, Muthukumar suggested that, if the excluded volume interaction is fully screened, the relaxation exponent for a polydisperse system can be expressed as:

$$n = \frac{d(d+2-2d_f)}{2(d+2-d_f)} \quad (22)$$

In the framework of eq. 22, all values of the scaling exponent $0 < n < 1$ are possible for a fractal in the physically realizable domain $1 < d_f < 3$. In the case of unscreened excluded volume interactions; $1 \leq n \leq 3/5$ as d_f varies from 1 to 3 (eq. 20 and 21). Incipient gel networks with high values of n , have low fractal dimensions and are said to be “open”, whereas networks with low values of n have higher fractal dimensions and are called “tight”. (See Figure 12)

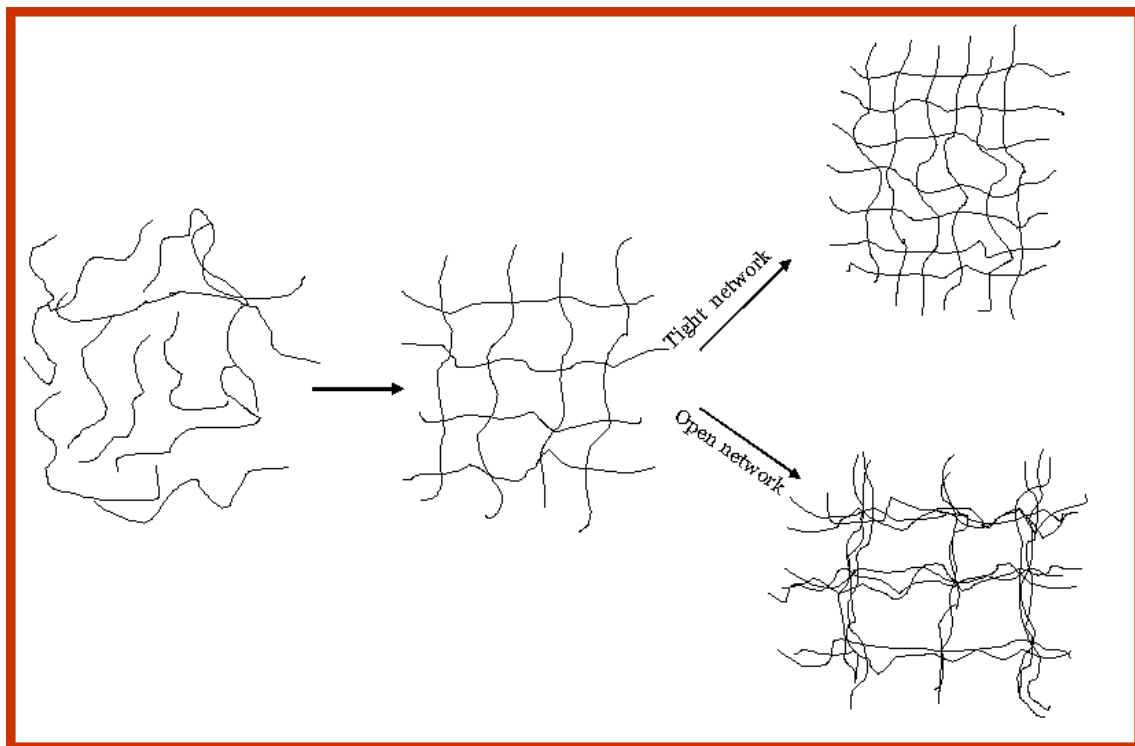


Figure 12. An illustration of an open and tight network.

Table 2 shows n value for different systems:

Table 2. A list of relaxation exponent for different systems

n	System
0.5	End-linking networks with balanced stoichiometry
0.5-0.7	End-linking networks with imbalanced stoichiometry
≈ 0.7	Epoxies
≈ 0.8	PVC plastisol
≤ 0.3	Radiation cross-linked polyethylene

It is evident from *Table 2*, that the value of the relaxation exponent can vary depending on the type of the system.²⁸

e) Stress Relaxation Experiments

In a relaxation experiment, the system is subjected to a fixed small strain, and the decay of the stress in the sample is probed as a function of time. This technique is applied on quite viscous samples with elastic properties, since in a viscous solution the relaxation is too fast and cannot be measured. However, some very rigidly cross-linked networks might not relax at all within a reasonable time scale.

The relaxation modulus, $G(t)$, follows a power-law behavior at the gel point³²:

$$G(t) = S \cdot t^{-n} \quad (23)$$

C. Small Angle Neutron Scattering (SANS)

The scattering process allows us to explore a system on a length scale of q^{-1} .

The wave vector q is defined as:

$$q = \frac{4\pi \cdot n_{ref} \cdot \sin(\theta/2)}{\lambda} \quad (24)$$

where λ is the wavelength, θ is the scattering angle, and n_{ref} is the refractive index of the solution. The same scattering equation can be used for a given value of q , regardless of whether visible light, neutrons or X-rays are employed in a scattering experiment. The information obtained from scattering depends on the quantity qL (where L is a characteristic length; R_g in the dilute regime or the screening length ξ in semidilute solutions), and there is an inverse relationship between the size of the scattering object and the q values at which scattering is observed. The value of the quantity qL indicates whether global ($qL < 1$) or local dimension ($qL > 1$) scales are probed.⁴⁵

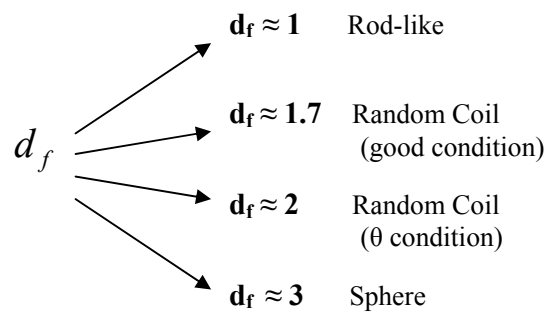
Small angle scattering (SAS) is the collective name given to the techniques of small angle neutron (SANS) and small angle X-ray scattering (SAXS). In each of these techniques, radiation is elastically scattered by a sample and the resulting scattering pattern is analyzed to provide information about the size, shape and orientation of some component of the sample. In addition, thermodynamic information may be extracted and enhanced aggregation or association of systems can be revealed at low q values.



Figure 13. Small angle neutron scattering (SANS) equipment at IFE.

Neutron radiation can be produced to cover a range of wave vectors $0.005 \leq q(\text{\AA}^{-1}) \leq 0.8$ (the SANS spectrometer at IFE), which makes the instrument able to probe the structure of the system on a more local scale. At large q ($qL \gg 1$) a power law is observed:

$$I(q) \propto q^{-d_f} \quad (25)$$



At low q value ($qL < 1$), a plateau can be observed, which is called the ‘Guinier regime’. In systems forming large association complexes, a strong upturn of the scattered intensity is observed at low q values that can be described by a power law:

$$I(q) \sim q^{-z}$$

In the ‘Porod Scattering’ regime, the value of the exponent is equal to $z = 4^{45-49}$, and it has been reported that the exponent can vary between 2 and 4. (See *Figure 14*)

Guinier approximation:

$$I(q) \propto \exp\left(-\frac{q^2 R_g^2}{3}\right) \quad (26)$$

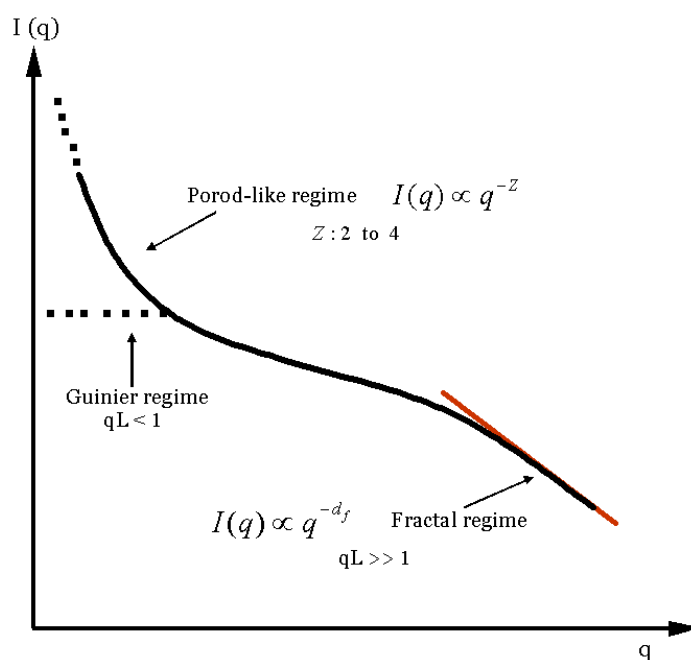


Figure 14. An illustration of the SANS scattering intensity over an extended q range.

D. Light Scattering

Light scattering has been used in this study as a method for determining polymer molecular weights, radius of gyration and some information about the mesh size of the network.⁵⁰ Both static (intensity) and dynamic light scattering are used to

determine these properties.⁵¹⁻⁵⁴ In this thesis, dynamic light scattering has been discussed, while the results from static light scattering are shown in *Table 3*. (See the appendix)

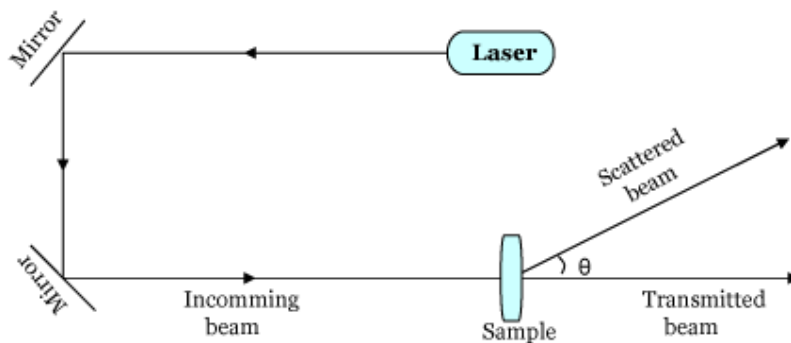
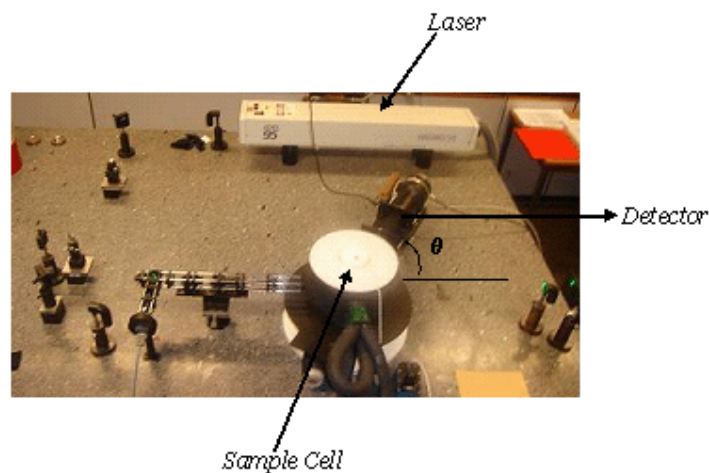


Figure 15. Light Scattering instrument of the Polymer Group at the University of Oslo (UiO), and a schematic illustration of it.

1. Dynamic Light Scattering (DLS)

A dynamic light scattering experiment probes the relaxation times of processes, which relax on some length scale q^{-1} . If the scattered field obeys Gaussian statistics, the measured homodyne intensity autocorrelation function, $g^{(2)}(q,t)$, can be related to

the theoretically amenable first-order electric field correlation function; $g^{(1)}(q,t)$, by the Siegert relation ⁵⁵:

$$g^{(2)}(q,t) = 1 + B|g^{(1)}(q,t)|^2 \quad (27)$$

where $B (\leq 1)$ is an empirical factor. The Siegert relation is valid under *ergodic* conditions; that is the time averaged intensity correlation function is equal to the ensemble averaged intensity correlation function. In other words, the decay curves of the time correlation function do not depend on the scattering position of the incident light in the sample. A frequent consequence of *non-ergodic* features is that the parameter B in the Siegert relation decreases; $B < 0.6$. In DLS studies of associating and gelling systems, it is usually observed ⁵¹, that the decay of the correlation function can initially be described by a single exponential, followed at longer times by a stretched exponential:

$$g^1(q,t) = A_f \exp[-t/\tau_f] + A_s \exp[-(t/\tau_{se})^\beta] \quad (28)$$

$$A_f + A_s = 1, 0 < \beta \leq 1 \quad (29)$$

where A_f and A_s are amplitudes for the *fast* and *slow* relaxation modes, respectively. τ_f is the fast relaxation time and τ_{se} is some effective slow relaxation time. β is a measure of the width of the distribution of relaxation times.

The mean relaxation time (τ_s) can be defined from the slow relaxation mode by:

$$\tau_s \equiv \int_0^{\infty} \exp\left[-\left(\frac{t}{\tau_{se}}\right)^\beta\right] dt = \frac{\tau_{se}}{\beta} \Gamma\left(\frac{1}{\beta}\right) \quad (30)$$

where Γ is the gamma function. The fast relaxation mode is a measure of how the whole network fluctuates and moves around, while the slow relaxation mode defines the movement of individual chains in the network.

The coupling model of Ngai⁵⁶ introduced the value of the coupling parameter (n_{coup}) related to the value of the stretch exponent (β) by:

$$\beta = 1 - n_{\text{coup}} \quad (31)$$

As the associations increase, the number of couplings in the network increases, and the stretch exponent (β) decreases. This model addresses the problem of how the relaxation of a specific chain or cluster is slowed down due to the interaction or coupling to complex surroundings, and it is in a good agreement with the results from several systems, as well as cross-linked semidilute HEC solutions.

The fast relaxation time can be determined by^{51,57}:

$$\tau_f^{-1} = D q^2 \quad (32)$$

where D is the diffusion coefficient (D_m , mutual diffusion coefficient in a *dilute* solution, and D_c , the cooperative diffusion coefficient in a *semidilute* system; a measure of how the collective polymer network fluctuates in the solution). The diffusion coefficients can be determined by:

$$D \cong \frac{k_B T}{6\pi\eta_0 X} \quad (33)$$

where k_B is Boltzmann's constant, ($1.38 \times 10^{-23} \text{ JK}^{-1}$), T is the temperature, η_0 is the viscosity of solvent. The quantity X is identified as ζ_h , the hydrodynamic correlation length, for *semidilute* solutions, which is a measure of the mesh size in the polymer network, and $X \equiv R_h$, the hydrodynamic radius, for *dilute* solutions.

The q dependency of the fast and slow mode can be expressed^{58,59} by:

$$\tau_f^{-1} \propto q^{\alpha_f}, \quad \tau_s^{-1} \propto q^{\alpha_s} \quad (34)$$

A diffusive mode is q^2 dependent.

IV. Experimental Section

In this study both dilute and semidilute samples have been examined by different experimental techniques.

A. Materials and Solution Preparation

A sample of hydroxyethylcellulose with the commercial name Natrosol 250 GR (Lot no. V-0403) was obtained from Hercules, Aqualon Division. The degree of substitution of hydroxyethyl groups per repeating anhydroglucose unit of the polymer is 2.5 (given by the manufacturer). Dilute HEC solutions were dialyzed against Millipore

water for at least 1 week to remove low molecular weight impurities. As a dialyzing membrane, regenerated cellulose with a molecular weight cutoff of 8000 (Spectrum Medical Industries) was used. After the dialysis, the samples were freeze-dried. After freeze-drying, the polymer was re-dissolved in aqueous alkaline (NaOH) media with pH of 11.8, and solution with the desired polymer concentrations were prepared by weighing the components and the solutions were homogenized by stirring at room temperature for one day.

The cross-linker agent, DVS, was purchased from Merck and utilized without further purification. Millipore water was used for the preparation of all solutions. Shortly before the commencement of experiment, the prescribed amount of DVS was added to the sample and a fast homogenization of the solution was performed. The same procedure to obtain homogeneous solutions was repeated for all samples to ensure good reproducibility of the measurements.

B. Turbidity Measurements

Time evolution of the transmittance of dilute and semidilute alkali solutions of HEC in the presence of various amounts of cross-linker (DVS) was measured with a spectrophotometer at a wavelength of 500 nm. The results will be presented in terms of turbidity (See eq. 1). For all samples, cells with 1 cm light path length have been used.

C. Rheology

Oscillatory sweep, stress relaxation and steady shear measurements were performed for semi-dilute samples, while for the dilute solutions only steady shear experiments were carried out. The cross-linker (DVS) was added to the HEC solution and the sample was homogenized during a short time and was then rapidly transferred to the plate and the measurements were started immediately. To prevent evaporation of the solvent, the free surface of the sample was always covered with a thin layer of low-viscosity silicone oil (the viscoelastic response of the sample is virtually not affected by this layer).

D. Small Angle Neutron Scattering (SANS)

The SANS measurements were performed on the SANS installation at the IFE reactor at Kjeller, Norway. These kinds of experiments were only performed on the semidilute samples, since the scattered intensity of the dilute samples is too weak to obtain a good enough signal. The wavelength was set by the aid of a selector (Dornier), using a high FWHM for the transmitted beam ($\Delta\lambda/\lambda = 20\%$), and maximized flux on the sample. The neutron detector was a 128x128 pixel, 59 cm active diameter, He-filled RISØ-type detector, which is mounted on rails inside an evacuated detector chamber. The samples were investigated in 2 mm Hellma quartz cells, using D_2O as a solvent to minimize incoherent scattering and to maximize the scattering contrast between the HEC and the solvent.

Standard reductions of the scattering data, including transmission corrections, were conducted by incorporating data collected from empty cell, beam without cell, and blocked-beam background to obtain the scattered intensities in absolute scale (cm^{-1}). Subtraction of the solvent scattering was then done to obtain the coherent macroscopic scattering cross section $d\Sigma/d\Omega(q)$ of the system, which is proportional to the scattered intensity ($I(q)$).

E. Dynamic Light Scattering (DLS)

The sample solutions were filtered through filters of different pore size (0.22 μm for dilute and 0.8 μm for semi-dilute solutions) into pre-cleaned 10 mm NMR tubes (Wilmad Glass Company) of highest quality. The full homodyne intensity autocorrelation function $g^2(t)$ was measured mostly at a scattering angle of 70° for dilute and 90° for semidilute solutions. All correlation functions were analyzed with the aid of eq. 28.

V. Results & Discussion

The results are presented in two sections: dilute and semidilute solutions. In this way, the presentation of the results should be more transparent.

A. Dilute Solutions

1. Turbidimetry

In *Figure 16* the time evolution of the turbidity for dilute HEC solutions at different cross-linker concentrations is depicted. It is evident that the solutions become turbid in the course of the cross-linking reaction at all cross-linking densities, except the lowest cross-linker concentration. The cloud point (CP) is the point at which a definite lack of clarity, cloudiness, appears in the solution, which is due to the decrease in the solubility of the polymer, caused by poorer thermodynamic conditions or aggregation. The cloud points can be determined by observing the start point of increasing in turbidity (See the inset plot). No cloud point is observed for the solution with the lowest cross-linker concentration. The turbidity results indicate that the formation of large aggregates starts at earlier times when the cross-linker concentration increases and the value of the cloud point time decreases as the level of cross-linker addition increases (See the inset). This finding demonstrates that, at quiescent conditions, the inter-polymer cross-linking behavior, with the formation of large aggregates, constitutes a dominant feature in the process. The generation of a microgel is assumed to take place through inter- and intrachain cross-linking. By intrapolymer cross-linking, microgel particles will formed. This process accompanies phase separation, and solution turbidity appears.²⁴

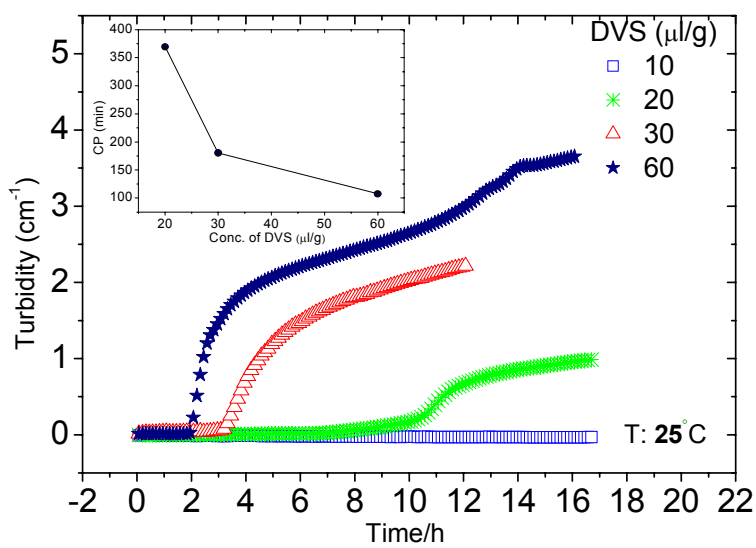


Figure 16. Time evolution of the turbidity (eq. 1) for 0.1 wt % HEC solutions with different cross-linker concentrations. The inset plot shows the values of the cloud point determined from the incipient rise of the turbidity curve.

2. Rheology

a) Intrinsic Viscosity and Huggins Coefficient

The intrinsic viscosity $[\eta]$ and Huggins coefficient k' can be determined from a measurement series on dilute polymer solutions. η_{sp} can be determined by eq. 3. The intrinsic viscosity $[\eta]$ and Huggins coefficient k' can be determined by plotting η_{sp}/c_p versus c_p :

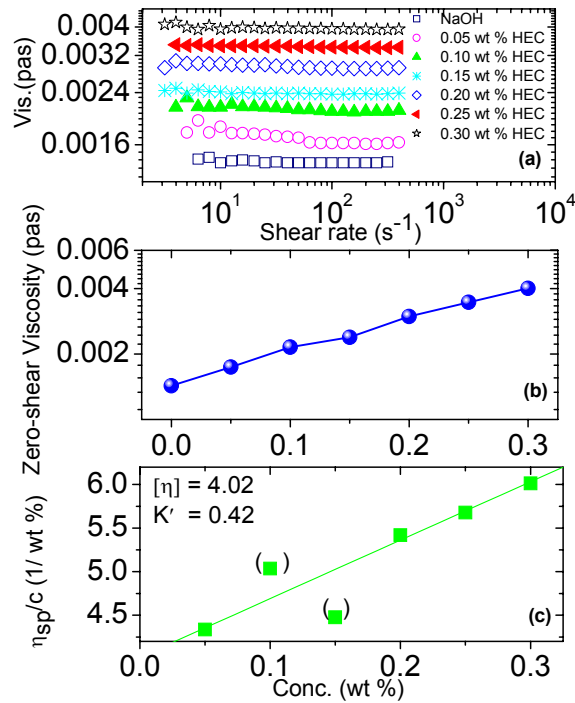


Figure17. (a) Plot of the viscosity as a function of shear rate for different polymer concentrations. (b) Plot of the zero-shear viscosity as a function of polymer concentration. The viscosity increases with increasing HEC concentration. (c) Plot of the reduced viscosity as a function of polymer concentration. The intrinsic viscosity and Huggins coefficient can be determined by using the eq. 6.

The overlap concentration C^* can be determined from eq. 35:

$$C^* = \frac{1}{[\eta]} \quad (35)$$

For the HEC solution in the presence of NaOH solvent ($pH \approx 11.8$), the overlap concentration is $C^* = 0.25$ wt %. This shows that the concentration (0.1 wt %) employed in the study on dilute solutions are well below C^* , while the concentrations (1 wt % and 2 wt %) utilized in the project on the formation of macroscopic gels are in the semidilute regime. The zero-shear viscosity increases with increasing the polymer concentration.

The value of Huggins coefficient ($k' = 0.42$) confirms the good thermodynamic condition of the system. ($k' < 0.5 \rightarrow$ good conditions)

b) Shear Viscosity Measurements

Figure 18 shows the time evolution of the viscosity for a reaction mixture of 0.1 wt % HEC and DVS of a concentration of 30 $\mu\text{l/g}$ under the influence of different shear rates. At the highest shear rate, the rotation and stretching of the chains induced by strong mechanical shear stresses prevent the intra- and inter-polymer cross-linking reactions from occurring, but slight increase of the viscosity at very long times may be a harbinger of incipient inter-chain aggregation. At lower shear rates, the general behavior is characterized by a minimum followed by a rise of the viscosity (a minimum of the transition area is depicted in the inset) at longer times. The former finding suggests contraction of the species and this behavior is a signature of intra-molecular cross-linking, whereas the latter feature announces inter-chain aggregation.

Intra-chain compaction of the molecules was never detected from the DLS measurements (see the discussion on DLS results below), probably because of the dominance of inter-polymer cross-linking at quiescent conditions.

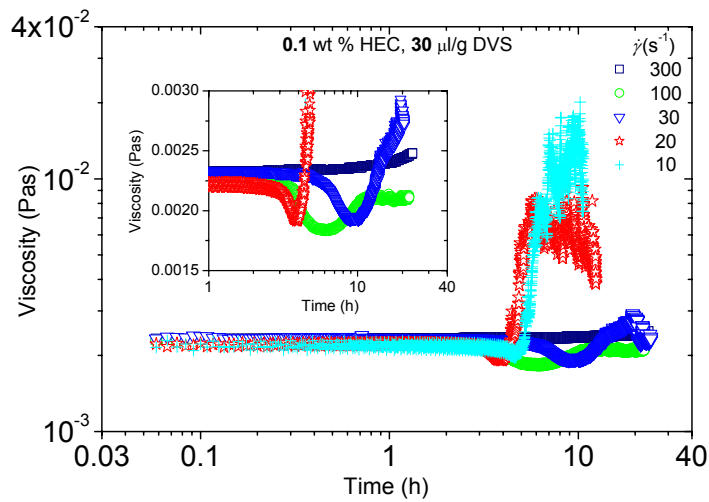


Figure 18. Time dependencies of the shear viscosity for a 0.1 wt % solution of HEC in the presence of 30 $\mu\text{l/g}$ DVS that is exposed to the shear rates indicated. The inset shows a magnification of the data around the transition zone.

At moderate shear rates, the rotation of the chains may initially be more favorable to intra-chain contacts than inter-chain reactions because the large number of hydroxyl groups on a single chain, and its rotational motion may facilitate intramolecular contacts and cross-linking. At longer times, the repeated collisions between the contracted species may lead to inter-polymer cross-linking reactions and the formation of multichain aggregates. A scrutiny of the magnitude of the viscosity raise for the lower two shear rates unveils that the breakup of the interconnected aggregates depends on the shear rate.

It is obvious from *Figure 18* that a lower shear rate promotes the buildup of larger clusters before rupture sets in. The scatter of the data points at the peaks of the viscosity curves signalizes the competition between the buildup and breakup of inter-aggregate chains when the complexes are sufficiently large. This size-limitation step

begins as soon as the aggregates reach a size large enough to be broken by the applied shear forces.

The enhancement of the viscosity takes place at earlier times at low shear rate and the steepness of the rise becomes weaker as the shear rate increases. This result is expected because at a lower shear rate inter-polymer association is promoted. A close inspection of the viscosity (η) enhancement at various shear rates discloses that the time dependence of the viscosity raise can be portrayed by a power law $\eta \propto t^\phi$ (See *Figure 19*). The inset plot shows that the raise of the viscosity becomes weaker as the shear rate increases. It can be argued that augmented shear rates should inhibit the growth of large association complexes since mechanical disturbances will obstruct the cross-linker reaction between functional groups on the polymer chains.

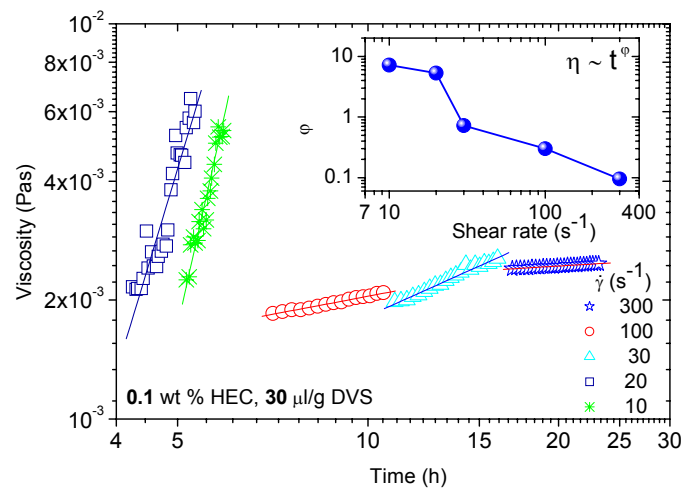


Figure 19. Time evolution of the shear viscosity in the regime where multichain aggregates are formed at the shear rates indicated for a 0.1 wt % HEC solution with 30 $\mu\text{l/g}$ DVS. The inset shows the shear rate dependence of the power law exponent ϕ , describing the time dependence of the viscosity ($\eta \sim t^\phi$) in the region of formation of inter-molecular aggregates.

In *Figure 20*, the time dependence of the viscosity at a constant shear rate (20 s^{-1}) for a 0.1 wt % HEC solution in the presence of different cross-linker concentrations is

depicted. The profile of the viscosity curves at the higher two DVS concentrations is similar to that observed above, that is, a minimum followed by an enhancement of the viscosity. The upturn of the viscosity takes place at an earlier time for the sample with the highest level of DVS addition, because the probability of forming inter-molecular cross-links is higher. A close inspection of the viscosity curves representing the two lower cross-linker densities reveals a decreasing tendency at long times, which may reflect an incipient intra-molecular cross-linking effect. In this case, the cross-linker concentrations are too low to provoke inter-chain aggregation over the time interval considered.

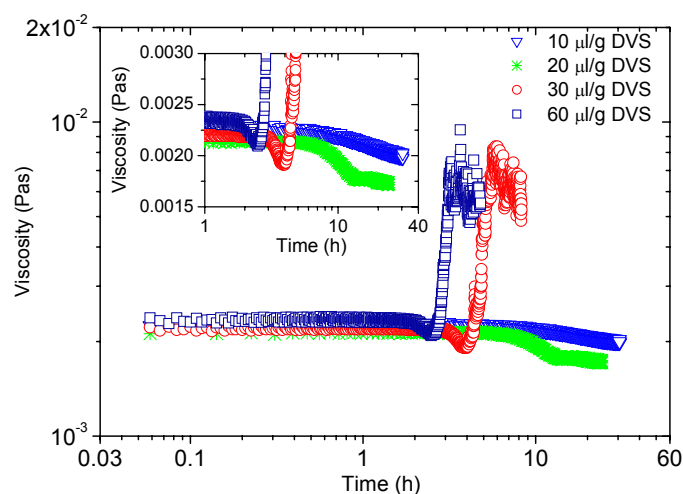


Figure 20. Time dependencies of the shear viscosity for 0.1 wt % solutions of HEC in the presence of the cross-linker densities indicated and at a shear rate of 20 s^{-1} . The inset shows a magnification of the data around the transition zone.

Figure 21 shows the time evolution of the viscosity at a fixed shear rate (20 s^{-1}), and a constant amount of DVS (30 μl/g) in solutions of different HEC concentrations. The general picture that emerges is that the polymer concentration plays an important role for the shear-induced development of intra-molecular and inter-molecular

structures. At the lowest HEC concentration, only a slight increase of the viscosity is visible at long times. This trend may be a message of incipient aggregation after several collisions of the entities.

At the higher two polymer concentrations, the general appearances of the viscosity curves are similar as discussed above, with a minimum and viscosity enhancement. The raise of the viscosity occurs at an earlier time for the higher polymer concentration, because the probability that inter-chain cross-links are developed is increased. The results in *Figure 21* show that the rheometer is capable to detect viscosity differences even between these low polymer concentrations. The average size of the inter-polymer complex before it disintegrates is larger for the highest polymer concentration. The conjecture is that a high polymer concentration promotes the creation of strong multi-chain aggregates.

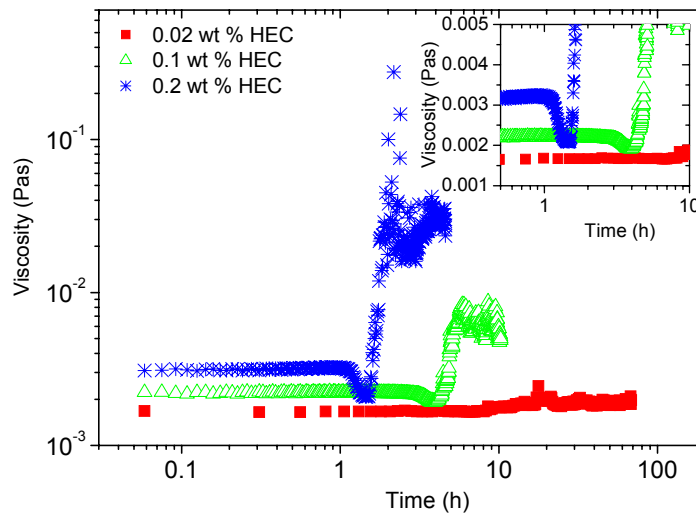


Figure 21. Time evolution of the shear viscosity during the cross-linker reaction for dilute solutions of HEC of the concentrations indicated in the presence of a cross-linker concentration of 30 $\mu\text{l/g}$ and at a shear rate of 20 s^{-1} . The inset shows a magnification of the data around the transition zone.

The time dependence of the viscosity at a constant shear rate (20 s^{-1}) and at the same HEC/DVS composition is illustrated in *Figure 22*. By keeping the value of the HEC/DVS ratio fixed, the state of the cross-linker reaction should be the same for all the samples. At the lower two polymer concentrations, only a slight decrease of the viscosity can be traced over time, but no inter-molecular association is visible. The reason is probably that the polymer concentration is too low to buildup inter-connected aggregates. At the higher polymer concentrations, compacted intra-molecular entities are formed and the subsequent creation and breakup of inter-aggregated chains are observed. Again the magnitude of the viscosity increases and a short induction time before the growth of the aggregates commences are promoted by a high polymer concentration.

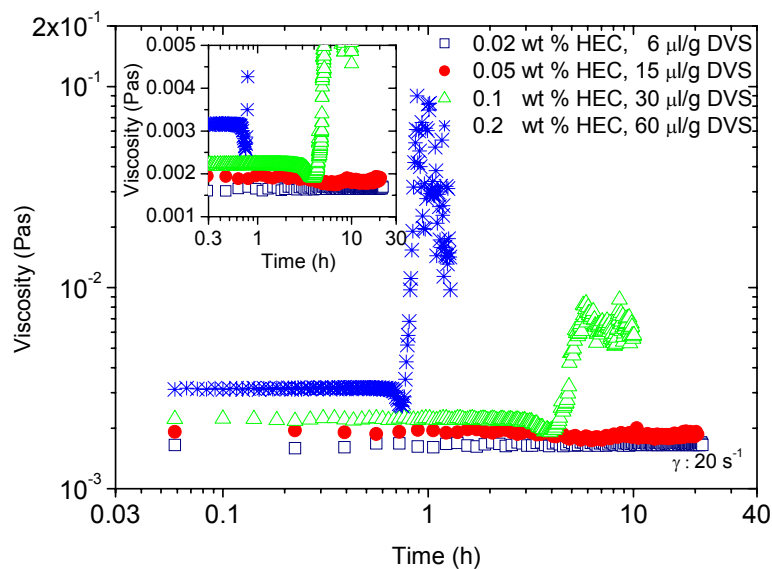


Figure 22. Time evolution of the shear viscosity during cross-linker reaction for mixtures of HEC and DVS at the cross-linker and polymer concentrations indicated and at a fixed shear rate of 20 s^{-1} . These compositions give a constant value of the HEC/DVS ratio. The inset shows a magnification of the data around the transition zone.

3. Dynamic Light Scattering (DLS)

a) Correlation Functions

Figure 23 shows the time evolution of the correlation function for alkali HEC solutions ($\text{pH} \approx 11.8$) of a polymer concentration of 0.1 wt % in the presence of different amounts of the cross-linker. The general trend is that the relaxation function is shifted toward longer times as the cross-linking process proceeds and this effect is more pronounced with increasing cross-linker concentration. The slower decay of the relaxation function at longer reaction times announces the growth of large clusters. The same effect has also been observed for other systems of different natures.^{51,60,61}

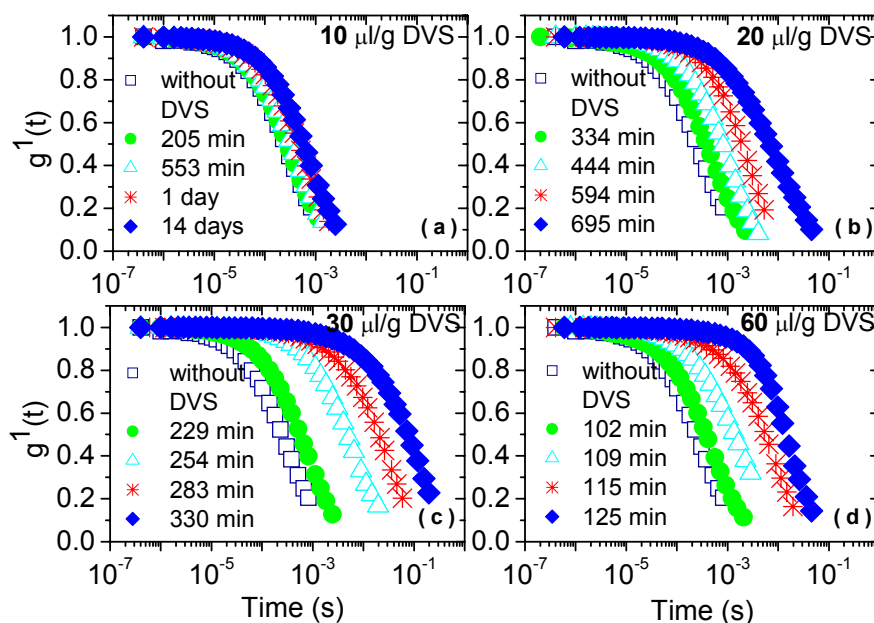


Figure 23. Plot of the first-order electric field correlation function versus time (every third data point is shown) at a scattering angle of 70° for 0.1 wt % HEC solutions with various cross-linker concentrations at different stages during the cross-linking reaction.

The growth of the aggregates has not been monitored over very long times in the light scattering experiments to avoid flocc sizes for which multiple scattering effects⁶³ may be significant (multiple scattering is usually observed in turbid samples). This effect is usually accompanied with a decrease of the value of B in the *Siegert* relation (eq. 27).

b) Fast and Slow Relaxation Times

The time dependencies of the reduced intensity (scattered intensity divided by the intensity of the incoming light) and the fast (τ_f) and the slow (τ_s) relaxation times are displayed in *Figure 24* for an alkali 0.1 wt % HEC concentration in the presence of various amounts of cross-linker. At the lowest DVS concentration, only a slight increase of the reduced intensity at very long times can be traced (*Figure 24a*), whereas for the other cross-linking densities abrupt upturns can be observed, suggesting that large association complexes are gradually formed. The rise of the reduced intensity occurs at earlier times when the cross-linker concentration increases. Similar trends are displayed for the relaxation times. The fast relaxation time probably reflects the motion of individual molecules and small associations of chains, whereas τ_s monitors the growth of large clusters. The growth of the aggregates starts at earlier times for high cross-linker densities and the rise of the relaxation times is stronger as the DVS concentration increases. These findings clearly demonstrate that at sufficiently high cross-linker concentrations, large inter-molecular complexes are evolved during the reaction in dilute alkali HEC solutions at quiescent conditions, and the kinetic features depend on the cross-linker concentration. This is expected, because at increasing level of cross-linker

addition the probability for inter-polymer associations is favored. The same trend has also been found for other systems.^{51,59,63}

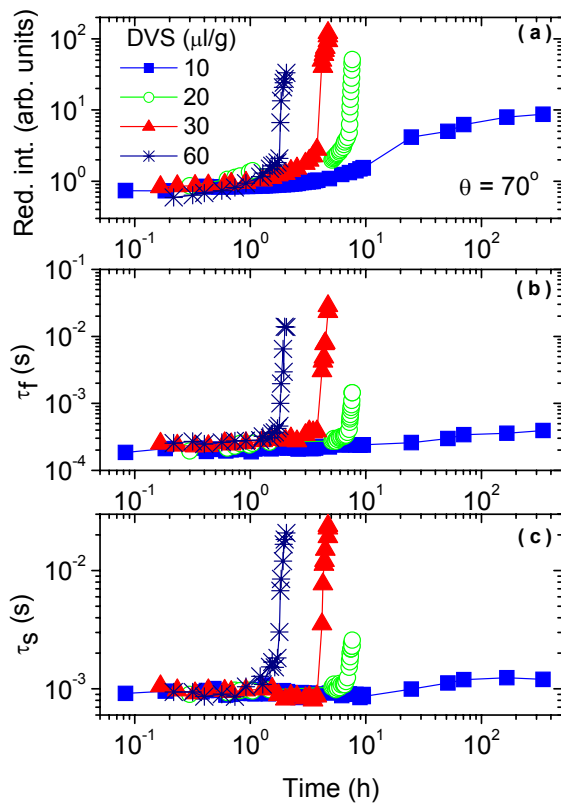


Figure 24. Time evolution of the reduced intensity, fast relaxation time, and slow relaxation time during the cross-linker process for a 0.1 wt % HEC solution in the presence of different amounts of cross-linker.

c) Quenching the reaction by HCl

To study the growth of the clusters under stationary conditions, 0.1 wt % solutions of HEC in the presence of a fixed amount of cross-linker (30 $\mu\text{L/g}$ DVS) were quenched by a rapid acidification of the reaction mixture at different stages during the association process, and the correlation functions were recorded (See *Figure 25a*). To scrutinize the fitting procedure and to endorse the functional form of eq. 28 that is used

to portray the correlation functions, residual plots at two different conditions for 0.1 wt % solutions of HEC are displayed in *Figure 25b*. The random distribution and small values of the residuals indicate good agreement between the fitting expression and the correlation function data. The results in *Figure 25c* show that the fast and the slow relaxation times increase with increasing quenching time, as well as the hydrodynamic radius (See the inset plot), calculated from the diffusion coefficient of the fast mode via the Stokes-Einstein relationship. These results demonstrate that the clusters grow as long as the cross-linker reaction continues.

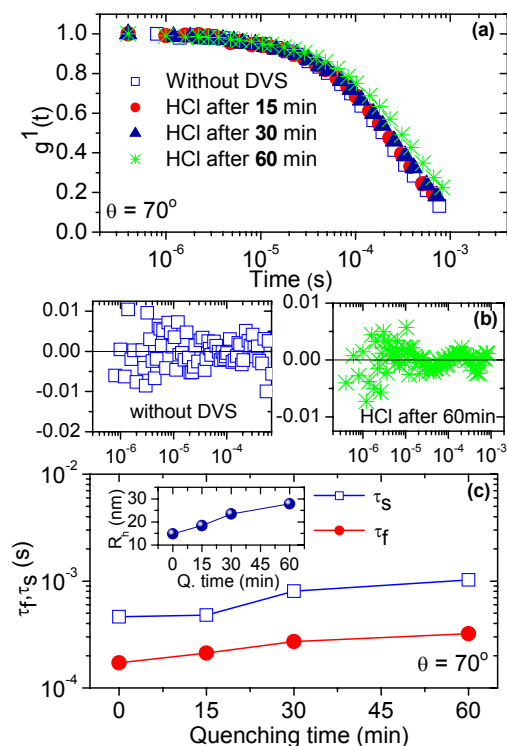


Figure 25. (a) First-order electric field correlation function versus time for 0.1 wt % HEC solutions without cross-linker and with 30 μ l/g DVS at different times of quenching (every third data point is shown). (b) Residuals obtained by fitting the correlation function data with the aid of eq. 28 at different stages of quenching. (c) Evolution of the fast and slow relaxation time at different times of quenching. The inset plot shows the effect of quenching time on the hydrodynamic radius (eq. 33), calculated from the fast relaxation time via the Stokes-Einstein relationship.

**(I) q Dependencies of the Fast
and Slow Relaxation Modes**

A diffusive mode is q^2 dependent. To define it more accurately, the power law parameter can be determined by eq. 34. As the cross-linking reaction demands a basic condition ($\text{pH} \approx 12$), it can be stopped by quenching with HCl and making a lower pH (≈ 1.5) in the solutions. The q dependencies of the correlation functions are demonstrated in *Figure 26* for the samples, which have been quenched at different times.

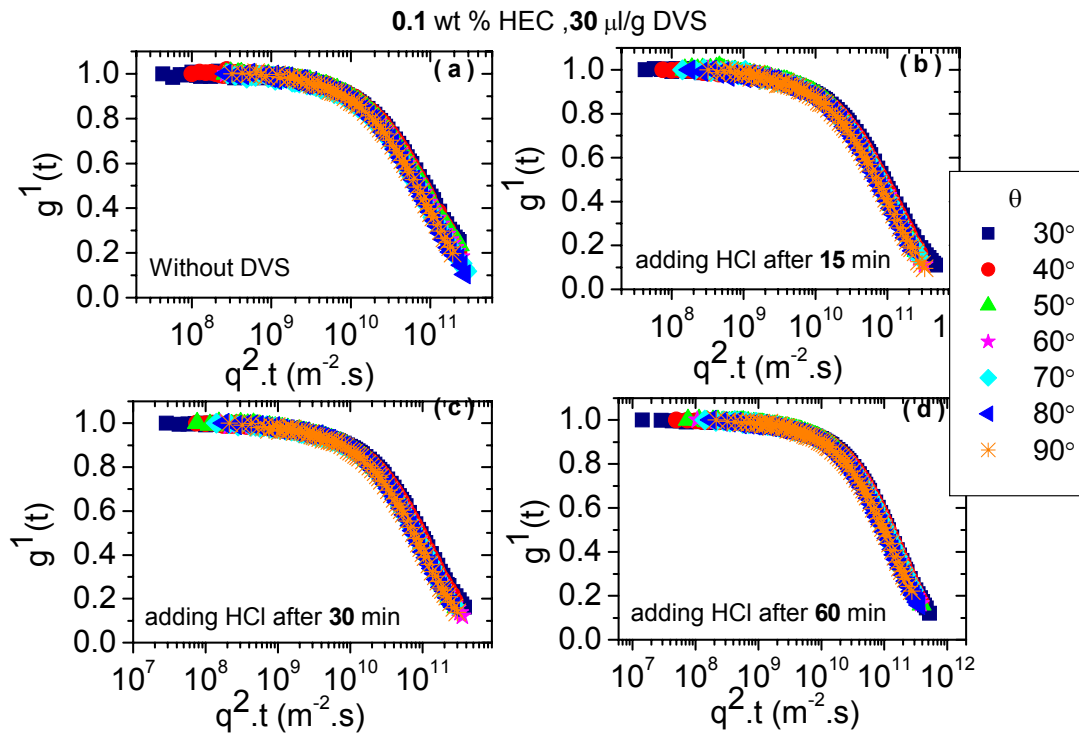


Figure 26. Plot of first-order electric field correlation function as a function of q^2t . The results show the q^2 dependency (diffusive mode) of the fast mode for the systems. As the cross-linking process proceeds, the q dependency of the slow mode is stronger than of a diffusive process.

By fitting the curves with the aid of eq. 28, and determining the fast and slow relaxation times, the inverse fast and slow relaxation times can be plotted as a function of q .

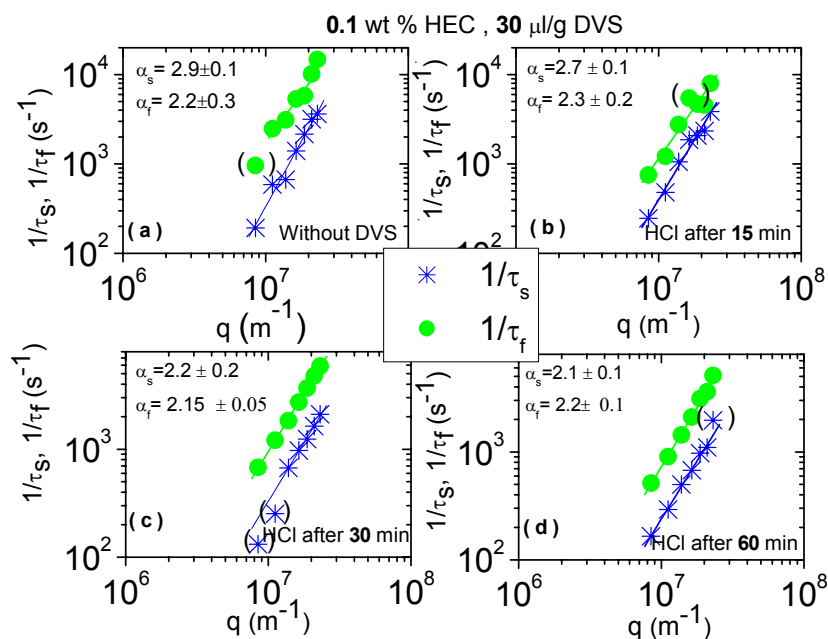


Figure 27. Plot of the inverse fast and slow relaxation time as a function of q .

For each curve, a straight line through the points of the different q values is fitted. The slopes of these lines yield values of α_f and α_s (cf. eq. 34). The results reveal that the fast relaxation process is always diffusive, and the slow mode is diffusive for the solutions with the two longest quenching times, whereas for the sample without DVS and the one quenched after 15 min a stronger q -dependence is observed. If the mode is diffusive, the mutual diffusion coefficient (D_m) can be determined. (eq.32).

(See Figure 28)

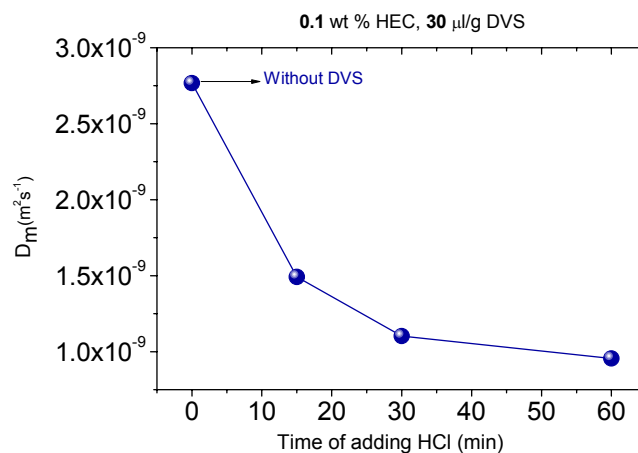


Figure 28. Plot of the mutual diffusion coefficient as a function of time of quenching for 0.1 wt % HEC in the presence of 30 μ l/g DVS.

As the cross-linking reaction proceeds (time of quenching increases), the mutual diffusion coefficient decreases, because of the formation of larger clusters.

(2) q Dependency of the Reduced Intensity

The q dependency of the reduced intensity for 0.1 wt % solutions of HEC is illustrated at different quenching times during the cross-linker reaction in *Figure 29*. In the limited q range covered in these measurements, the wave vector dependency of the reduced intensity I_{red} can be described by a power law $I_{red} \sim q^{-1}$, where the value of the scaling exponent may reflect the rod-like behaviour of the semi-rigid polysaccharide chains⁶⁴. It is interesting to note that the value of the exponent does not vary as the association complex grows, which suggests that on this dimensional scale the structure is not affected by the inter-polymer cross-linking process. The inset of *Figure 29* shows that the reduced intensity rises strongly with the quenching time, announcing significant

inter-chain aggregation and increased molecular weight of the clusters because for a given polymer concentration the reduced intensity is proportional to M_w .

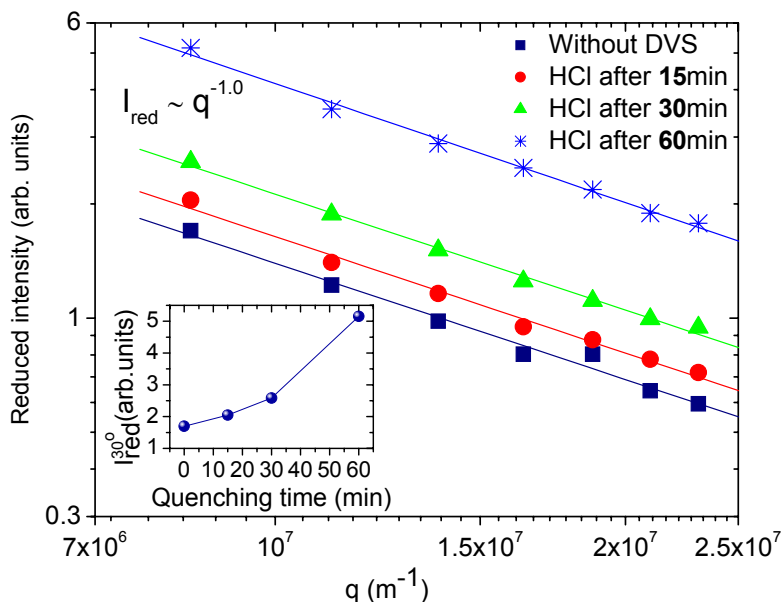


Figure 29. Wave vector dependencies of the reduced intensity for 0.1 wt % HEC solutions without cross-linker and with 30 μg /g DVS at different times of quenching. The inset shows the reduced intensity at a scattering angle of 30° at different times of quenching.

To examine whether the aggregation process continues after quenching arrested the cross-linking reaction, correlation functions were recorded over a long time (*Figure 30*). It was suspected that the quenched species might possess an enhanced stickiness that could lead to further aggregation. However, the collapse of the correlation function data onto a single curve suggests that the quenched clusters exhibit no tendency to further associate into larger complexes. This means that decrease of pH is an efficient method to interrupt the inter-chain aggregation process.

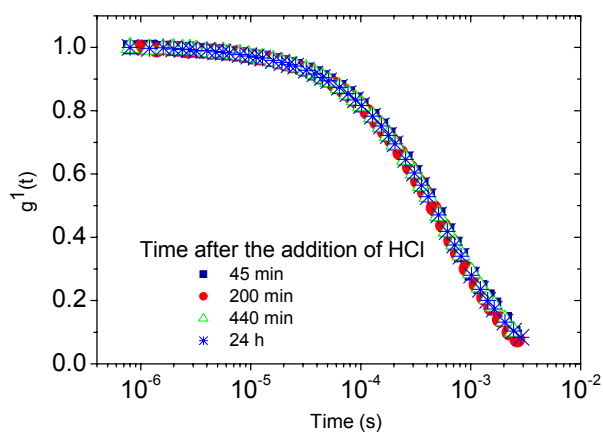


Figure 30. First-order electric field correlation function versus time for a 0.1 wt % HEC solution with 30 $\mu\text{l/g}$ DVS (every second data point is shown). The correlation functions have been recorded over a long time after the sample was quenched. This demonstrates that no further aggregation takes place after quenching.

B. Semidilute Solutions

1. Turbidimetry

In the post-gel region, all gels exhibit syneresis effects, that is, the strong shrinkage of the gel samples over time cause expulsion of solvent. A systematic examination of this de-swelling effect is in progress⁶⁵. An illustration of this effect is displayed in *Figure 31*:



Figure 31. An illustration of gel shrinkage and appearance of turbidity during the cross-linker reaction of 1 wt % HEC sample with a DVS concentration of 15 $\mu\text{l/g}$.

In the analysis of the time evolution of the gelation process it is convenient to introduce the quantity ε , which is the relative distance from the gel point and can be defined by:

$$\varepsilon = \frac{t - GP}{GP} \quad (36)$$

where t is the reaction time and GP is the gel point (for the determination of the gel point, see the discussion in section 2b(3) below).

The degree of turbidity depends on both the cross-linker concentration and the distance from the gel point (See *Figure 32*). The growth of the turbidity is promoted by high cross-linker concentration, and the cloudiness of the gel increases in the post gel region during a long period of time after the formation of the gel.

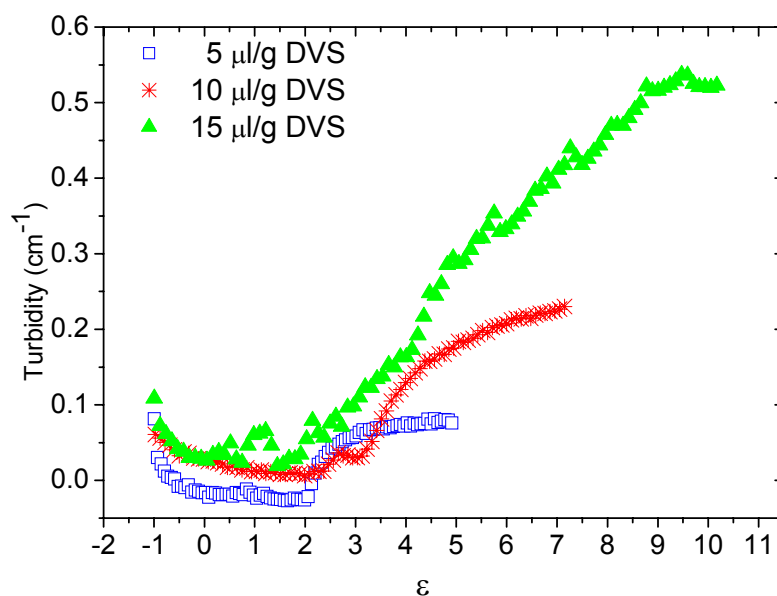


Figure 32. Time evolution of the turbidity for 1 wt % HEC solutions with the cross-linker concentrations indicated. Every 15 data point is shown.

The turbidity starts to increase in the post-gel region for all polymer solutions. It is shown in *Figure 31 and 32* that the samples are very clear at the gel point ($\epsilon = 0$), and some time after the gel point. The samples in the post-gel become more turbid as the concentration of DVS increases, which is due to the larger cross-linking zones in the presence of higher amount of the cross-linker at a constant polymer concentration. The same results have been found for other systems.⁴

According to the cross-linking mechanism mentioned above (*Figure 5*), the cross-linking reaction proceeds at basic condition, therefore the growth of the turbidity can be quenched at an earlier stage by adding a few drops of concentrated HCl to the samples to lower the pH to acid conditions ($\text{pH} \approx 1.5$) and thereby terminate the cross-linker reaction.

2. Rheology

a) Steady Shear Measurements

Steady shear measurements have been conducted on 4 different concentrations of HEC in the semidilute regime. When the shear rate is raised and then lowered again, for some systems, it takes time to re-arrange, and as a result hysteresis effects may arise.

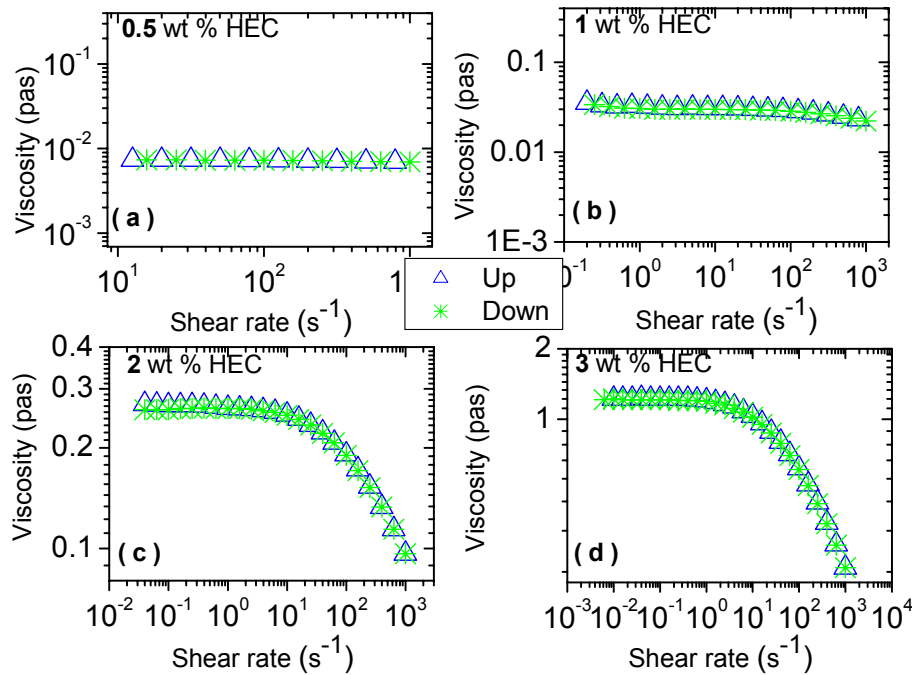


Figure 33. Plot of viscosity as a function of shear rate for different HEC concentration. The curves showed with stars (*) are measured from low to high shear rates, while the curves showed with triangles (Δ) are measured from high to low shear rates. Every second data point is shown.

It is evident from *Figure 33* that the hysteresis effect is small for all the considered polymer concentrations, which suggests that no complex association structures are formed. The shear rate dependency of the viscosity for all the systems has been determined by finding the slope of the curves at high shear rate, using eq. 2. (See *Figure 34c*)

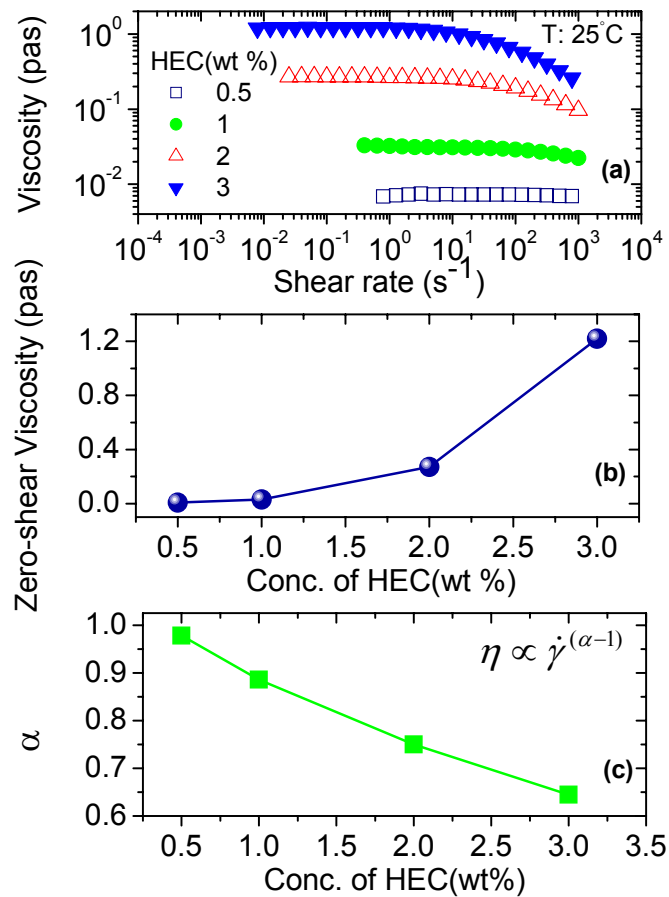


Figure 34. (a) Plot of viscosity as a function of shear rate for different HEC concentrations. Every second data point is shown. (b) Plot of Zero-shear viscosity as a function of polymer concentration. (c) Plot of the power law index as a function of polymer concentration. According to eq.2, the system shows shear thinning effect in all conditions, and it is more pronounced for the higher HEC concentrations.

The zero-shear viscosity increases with increasing the polymer concentration. (Figure 34b). For the two lower polymer concentrations (0.5 wt % and 1 wt %), Newtonian behavior is observed, whereas for the higher two concentrations of HEC solutions (2 wt % and 3 wt %), Newtonian behavior is observed at low shear rate, and the shear thinning effect is found at higher shear rates. The decreasing trend of α in Figure 34c, which has been plotted with the aid of eq. 2 shows that the shear thinning

effect is stronger for higher polymer concentrations. Because of enhanced associations and more entanglements in the solutions at higher polymer concentration, the effect of breaking them up at high shear rate is more pronounced.

The same measurement has been performed for a constant polymer concentration (1 wt % HEC) at different temperatures. (See *Figure 35*)

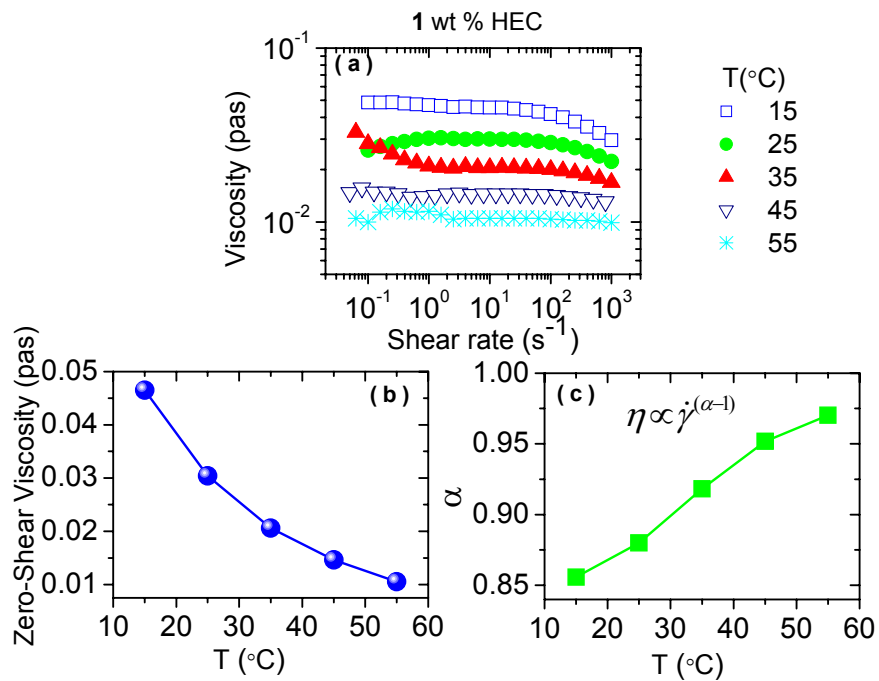


Figure 35. (a) Plot of viscosity as a function of shear rate for 1 wt % HEC concentration at different temperatures. Every second data point is shown. (b) Plot of zero-shear viscosity as a function of temperature. (c) Plot of the power law index as a function of temperature.

Because the mobility of the polymer chains increases with increasing temperature the viscosity decreases. The shear thinning behavior has also been observed for other systems with different conditions.³⁰

b) Oscillatory Shear Measurements

The viscoelastic behavior of the system has been examined for 4 different HEC concentrations. (See *Figure 36*)

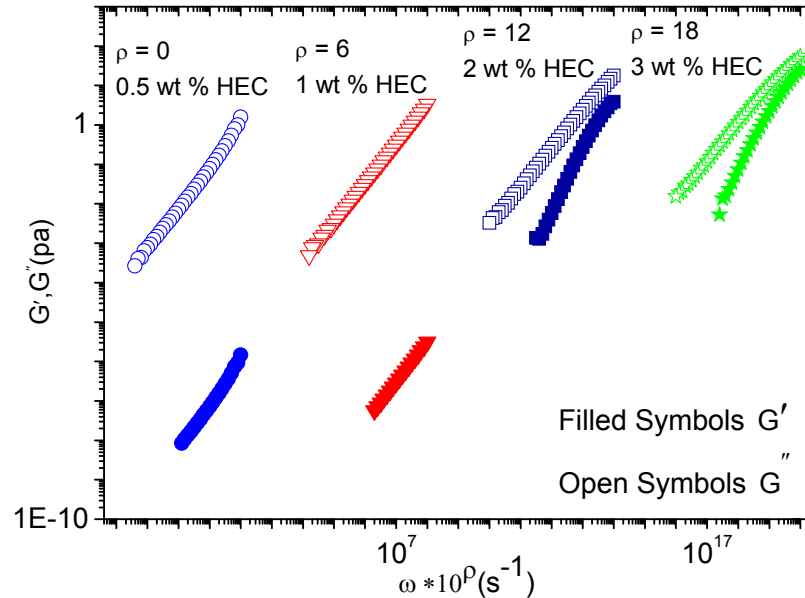


Figure 36. Frequency dependencies of the storage modulus G' and the loss modulus G'' for the systems indicated. The curves have been shifted horizontally by a factor ρ of the value mentioned in the graph.

For the lowest polymer concentration, the loss modulus is much higher than the storage modulus, and the distance between the storage and loss modulus becomes less and less by increasing the HEC concentration, which shows a higher contribution of the elastic response as the polymer concentration rises. These results reveal that the viscoelastic behavior becomes stronger as the concentration of polymer increases, due to the stronger interactions and formation of entanglements in the system.^{3,66}

(I) Angular Frequency Dependency of the Complex Viscosity

The frequency dependency of the absolute value of the complex viscosity has been examined for HEC solutions of different concentrations. (See *Figure 37*)

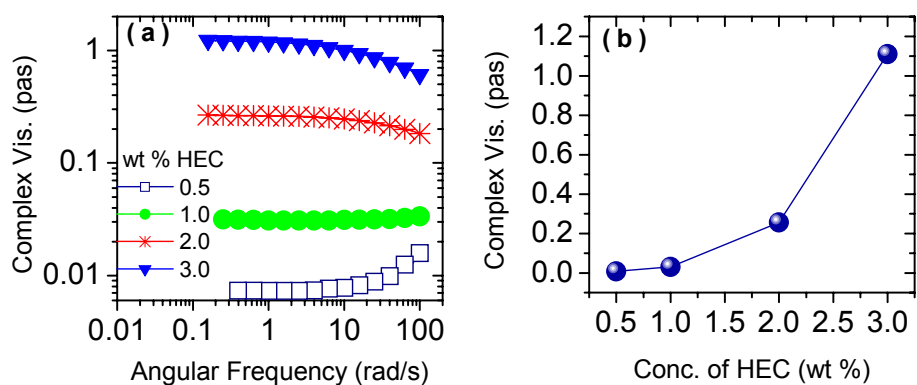


Figure 37. (a) Frequency dependencies of the complex viscosity for different HEC concentrations. Every second data point is shown. (b) Plot of the complex viscosity as a function of polymer concentration at a constant value of the angular frequency ω (3.98 rad/s).

The complex viscosity at a low value of the angular frequency rises as the polymer concentration increases (*Figure 37b*), and at higher values of angular frequency, shear thinning effect is observed for the two higher concentration of HEC (2 wt % and 3 wt %), while turbulence⁶⁷ (the upturn in viscosity at high angular frequencies) can be seen for the lowest concentration (0.5 wt %). The viscosity of the 1 wt % HEC solution (the concentration that is focused on in this thesis) is almost plateau-like, showing a Newtonian behavior.

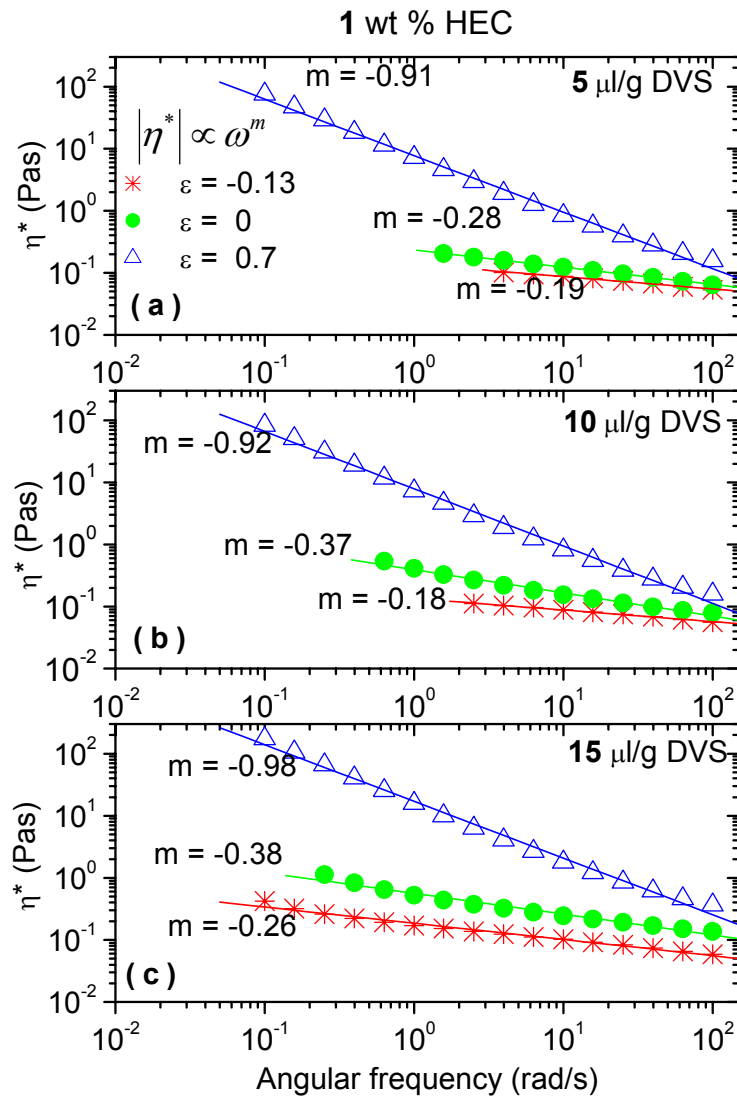


Figure 38. Frequency dependencies of the absolute value of the complex viscosity (η^*) at different stages during the gelation process of 1 wt % HEC solutions with different levels of cross-linker addition.

The frequency dependence of the absolute value of the complex viscosity, as measured in small amplitude oscillatory shear experiments, at different stages during the gelation process for a 1 wt % HEC solution at different cross-linker concentrations is displayed in *Figure 38*. The general trend is that at early stages in the pre-gel domain, weak frequency dependence of $|\eta^*|$ is found (liquid-like behavior), whereas as

the gel evolves, a progressively stronger dependence is observed and a solid-like response is approached for gels far into the post-gel region. A higher cross-linker concentration favor the growth of more effective intermolecular bridges during the cross-linking reaction, and a stronger gel beyond the gel point with an almost solid-like response (m close to -1) is found. These results clearly show that the chemical cross-linking reaction in HEC solutions proceeds far beyond the gel point. The same trend for the value of m has also been found for other systems.^{4,34}

(2) Testing of the Cox-Merz Rule

According to the Cox-Merz rule⁶⁸, the viscosity as a function of shear rate is identical to the complex viscosity as a function of frequency, f ($\omega = 2\pi f$). Deviations from this rule are often observed for more complex polymer systems. (See *Figure 39*)

At very low frequencies/shear rates, no difference between the methods is observed. However, as the polymer concentration is increased there is a deviation at higher frequencies/shear rates between the complex viscosity and the shear viscosity. The most pronounced deviations from the Cox-Merz rule are observed for the most entangled solutions. This type of behavior has been reported for many associating polymer systems that display shear thinning effect.⁶⁹

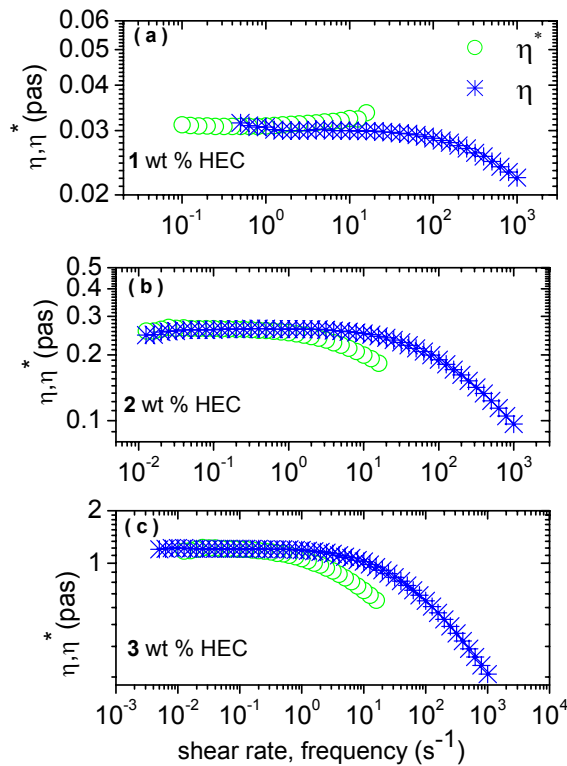


Figure 39. Plot of viscosity as a function of shear rate and the complex viscosity as a function of frequency for three different HEC concentrations.

(3) Determination of the Gel Point

In a semi-dilute solution of HEC in the presence of a sufficiently amount of the cross-linker DVS, the system will gradually form a gel. The gel point can be determined³⁴ by observation of a frequency-independent value of $\tan \delta$ ($= G''/G'$) obtained from a multi-frequency plot of $\tan \delta$ versus time. The gel point has been determined for two different HEC concentrations (1 wt % and 2 wt %) with different amounts of divinylsulfone (DVS) as a cross-linker. For the sample with 1 wt % HEC, 3 different concentrations of DVS (5, 10 and 15 $\mu\text{l/g}$) have been added to the polymer

solution (Figure 40), while for the 2 wt % HEC, the measurement has been done by adding only 5 $\mu\text{l/g}$ DVS to the sample.(Figure 41)

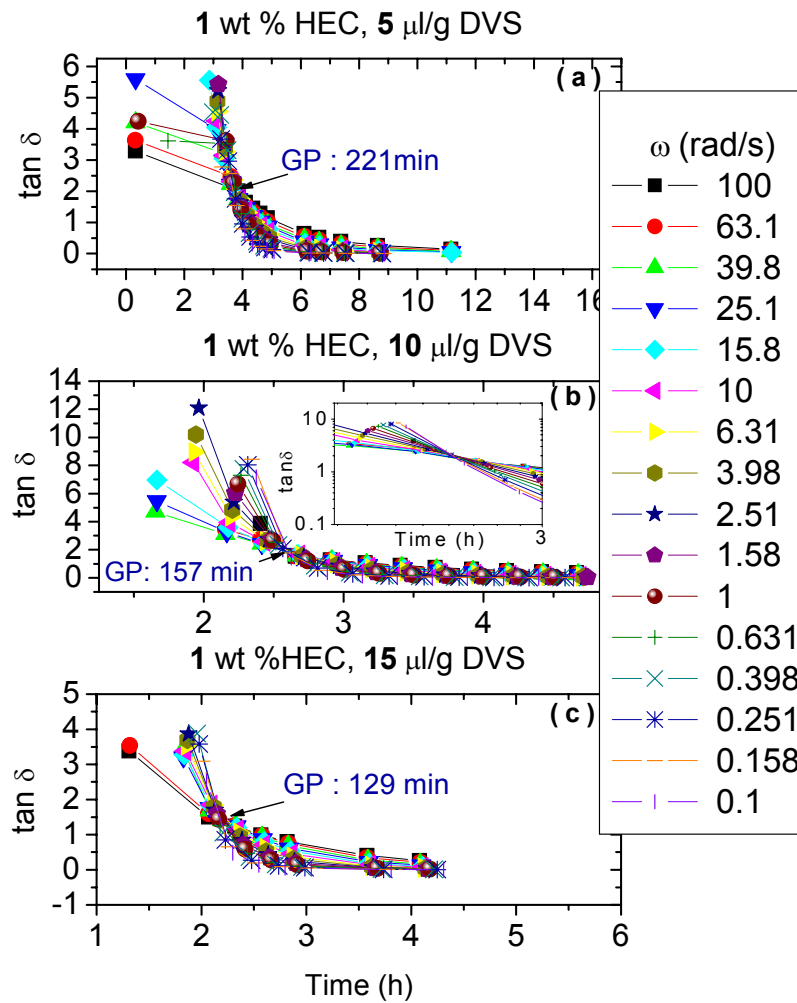


Figure 40. Time dependency of $\tan \delta$ at various angular frequencies for 1 wt % HEC solutions in the presence of different cross-linker concentrations; (a) 5 $\mu\text{l/g}$ DVS, (b) 10 $\mu\text{l/g}$ DVS, (c) 15 $\mu\text{l/g}$ DVS. At the gel point, $\tan \delta$ is frequency independent. The gel points (GP) are indicated. The inset plot of Figure 40b shows the magnification of the area around the intersection.

The gel point decreases as the concentration of the cross-linker increases, because the probability of cross-linking increases and enhanced cross-linking zones

evolve. The polymer concentration plays also an important role in the gelation process, and gelation occurs at earlier times (cf. *Figure 41*) as the polymer concentration is increased because more reaction sites are available for intermolecular cross-linking. The same results have also been found for other systems.³

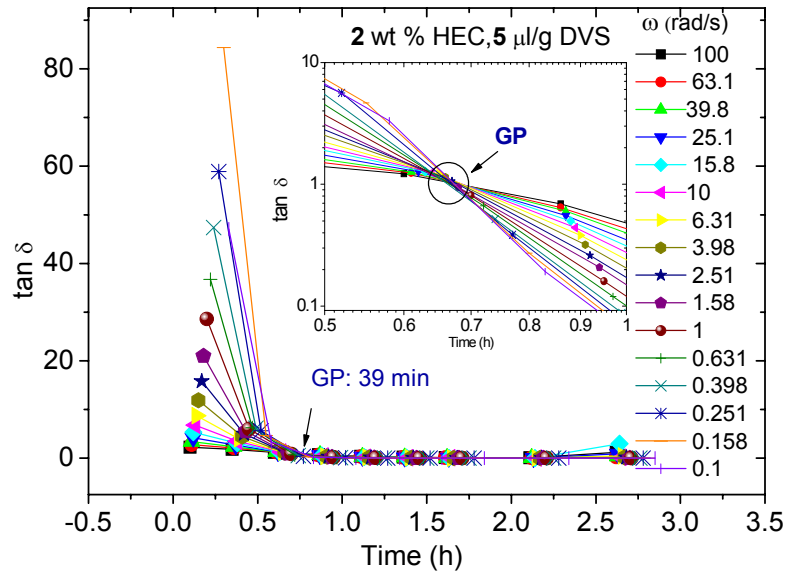


Figure 41. Viscoelastic loss tangent ($\tan \delta$) as a function of time for 2 wt % HEC solution with a cross-linker concentration of 5 $\mu\text{l/g}$ DVS. The inset plot shows the magnification of area of intersection.

Figure 42 shows the angular frequency independency of $\tan \delta$ at the gel point for 1 wt% HEC with different DVS concentration. Since $\tan \delta$ is independent of the angular frequency³ at the gel point ($\varepsilon = 0$), the plateau is observed at this point by plotting $\tan \delta$ versus ω . Depending on the viscoelastic behavior of the solution and the relation between storage (G') and loss modulus (G''), the value of $\tan \delta$ is different for different systems. In the present work, the value of loss modulus is always larger than

the storage modulus (*Figure 44*) at the gel point. As a result $\tan \delta > 1$ (eq. 10) is observed for all HEC solutions in the presence of different DVS concentrations.

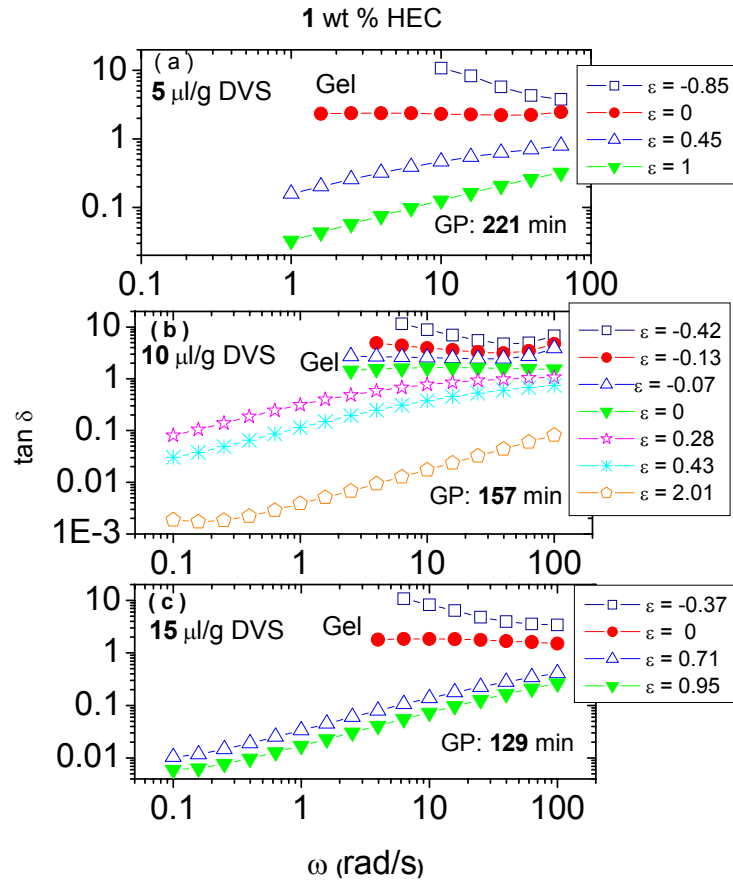


Figure 42. Plot of $\tan \delta$ versus angular frequency (ω) for 1 wt % HEC in the presence of different cross-linker concentrations. The graph at the gel point is independent of ω .

An alternative method^{3,32} to determine the gel point is the observation of the crossover of n' and n'' (eq. 14) (See *Figure 43*). The results from this procedure are in a very good agreement with the results from the observation of the crossover of $\tan \delta$ versus ω (*Figure 41*). The same agreement is also observed for incipient gels with 1 wt % HEC with different DVS concentrations.

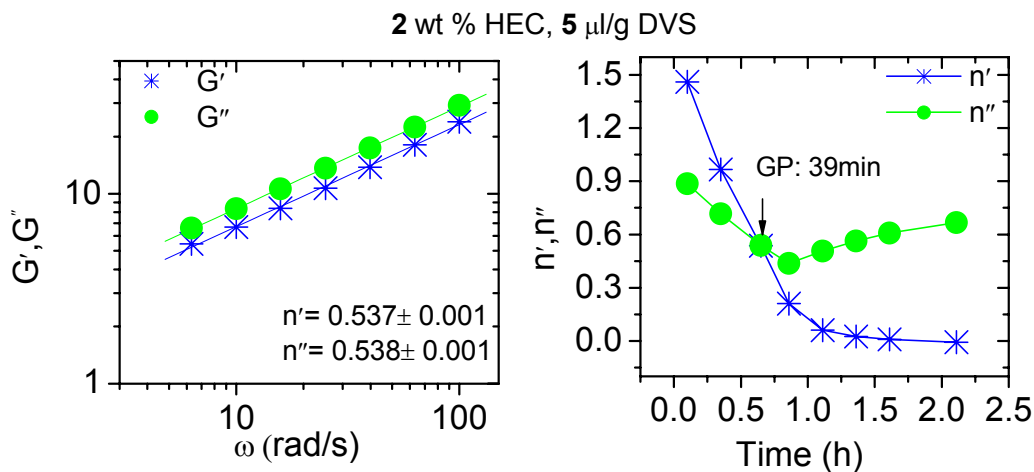


Figure 43. (a) Frequency dependencies of the storage and loss modulus for 2 wt % HEC with 5 $\mu\text{l/g}$ DVS at the gel point, showing the power law behavior. (b) Time dependency of n' and n'' during the gelation.

The lower value of the relaxation exponent (n) for 2 wt % HEC as compared with 1 wt % HEC at the gel point (*Figure 45*), support the hypothesis of enhanced associations and more entanglements in the system with the higher polymer concentration.³² The same features have also been found for other systems.^{3,66}

Up to the gel point, G' is always smaller than G'' , and liquid-like behavior is observed. After the gel point, G' becomes larger than G'' , which is a characteristic feature of the elastic response that is dominant in the post-gel region. The elastic response in the post-gel domain becomes stronger as the cross-linker concentration increases. (See *Figure 44*)

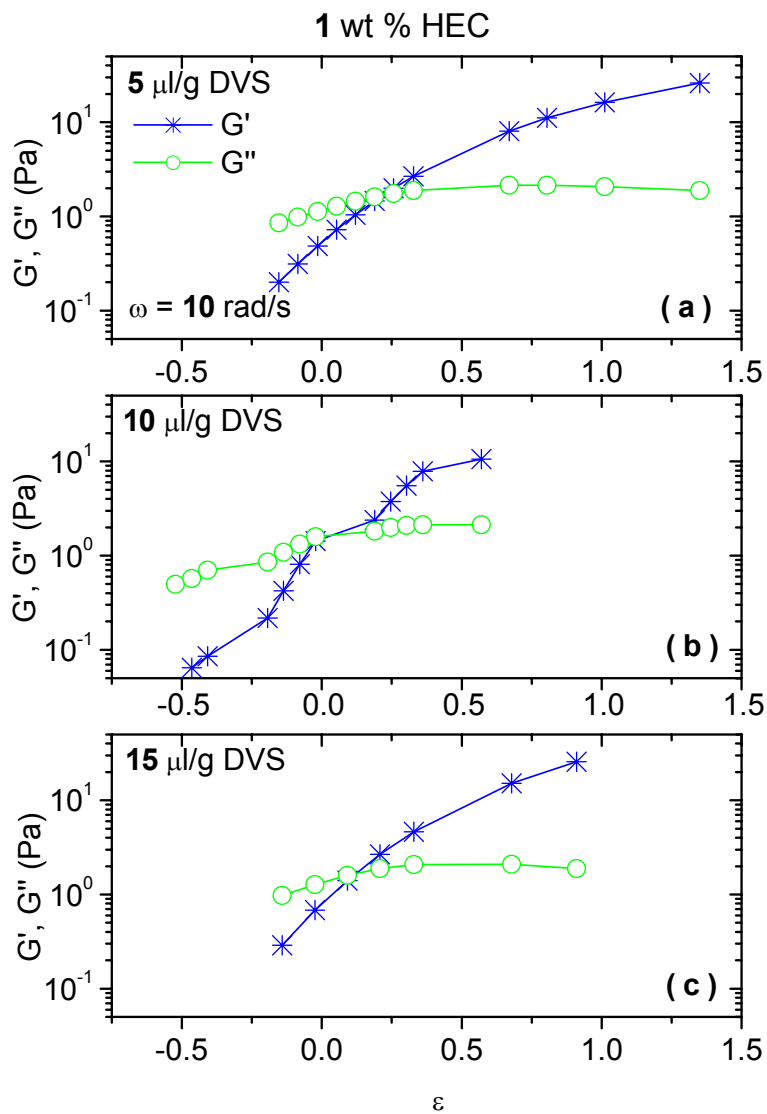


Figure 44. Plot of the storage and loss modulus as a function of ε (eq. 36) for 1 wt % HEC solution in the presence of different amounts of DVS. The loss modulus is higher than the storage modulus at the gel point ($\varepsilon = 0$).

(4) Gel Strength Parameter (S)

and the Relaxation Exponent (n)

Effects of cross-linker concentration on the gel point, n, and S for incipient gels (1 wt %) are illustrated in *Figure 45*. The incipient gel is formed when the connectivity

of the sample-spanning network has been established. The time of gelation decreases as the level of cross-linker addition increases. This suggests that the number of ‘active sites’ for cross-linking of the polymer network increases. It has been observed^{3,4,51} that both increasing cross-linker density and polymer concentration favor a faster gelation, because the kinetics of gel-formation is controlled by the probability of forming cross-links in the system.

The values of n (≈ 0.7) observed for the present incipient gels at different cross-linker concentrations (See *Figure 45b*), are consistent with the percolation model^{37,38,70}, which describes the fraction of chemical bonds at the gel point to establish the connectivity of a sample-spanning cluster. This finding is parallel with that reported^{3,4,33,71} for other incipient gels that have been chemically cross-linked. The gel strength parameter (calculated from eq.15 in combination with eq.17) is found (*Figure 45c*) to rise steadily with increasing level of DVS addition. This is intuitively expected, because a higher cross-linker concentration should promote a more efficient cross-linked network with higher gel strength. It has been observed^{3,4,26} for other gelling systems that at higher polymer concentrations, where the polymer entanglements contribute to the strength of the network, the excess of cross-linker concentration has reduced the impact on the gel strength parameter and a value of n lower than 0.7 is usually reported.⁷⁰

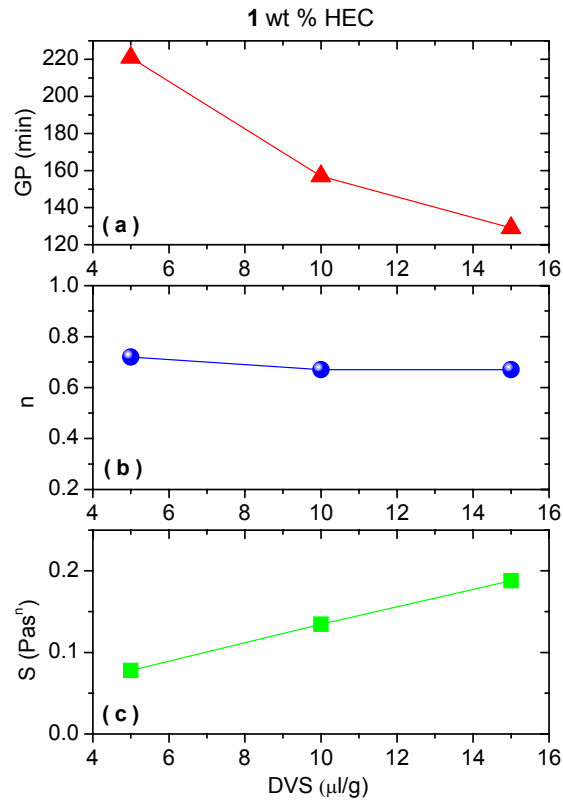


Figure 45. Effect of cross-linker concentration on the gel point, exponent n (eqs.15 and 16), and the gel strength parameter (eq.15) for incipient gels of 1 wt % HEC solution in the presence of various cross-linker concentrations.

(5) Zero-Shear Viscosity

Figure 46 shows the evolution of the shear viscosity at low shear rates in the course of gelation of a 1 wt % HEC solution in the presence of 10 $\mu\text{l/g}$ DVS. To probe the viscosification of the system during the gelation process, the value of the shear rate was continuously lowered as the gelation proceeds to monitor an apparent zero-shear viscosity. At the gel point, a sharp transition of the viscosity to higher values is observed. The pronounced viscosity enhancement beyond the gel point announces the development of a strong gel network. The strengthening of the network proceeds over

a long time, and the scattering of the viscosity values detected at long times may reflect effects of syneresis (See the discussion above). As a result of this effect, solvent is expelled from the gel sample and this may lead to slippage during measurement and scatter of the viscosity values. These results demonstrate that it is possible to probe the evolution of the gel by steady shear measurements if the magnitude of the shear rate is adjusted as the viscosification of the system is enhanced. This is the first time this is demonstrated.

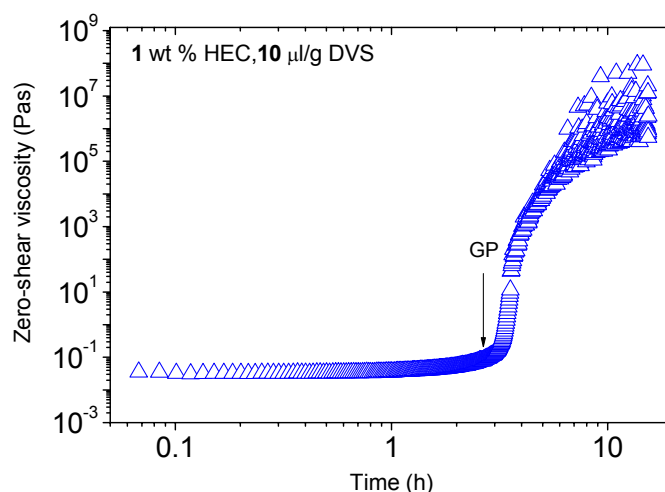


Figure 46. Time evolution of the apparent zero-shear viscosity during the gelation of 1 wt % HEC solution at a cross-linker concentration of 10 µl/g. The shear rate has continuously been shifted toward lower values to be in the apparent zero-shear regime.

c) Stress Relaxation Experiments

The decay of the relaxation mode (determined from stress relaxation measurements) is shown in *Figure 47* for a cross-linker concentration of 10 µl/g. Similar results are observed at the other considered cross-linker concentrations. Up to the gel point the relaxation process is so fast that it is not possible to monitor it with a mechanical technique such as rheology. In the post-gel region the slow decay can be

captured, and at sufficiently large values of ε almost no relaxation of $G(t)$ is detected in the considered time window. *Figure 47c* shows the change of the initial relaxation modulus $G(i)$ during the gelation process. The results demonstrate that beyond the gel point the elastic response increases because more cross-links are established in the post-gel region. The gel network is strengthened during a long time after the gel point, and a more solid-like material evolves. The same results have been found for other systems.^{32,57}

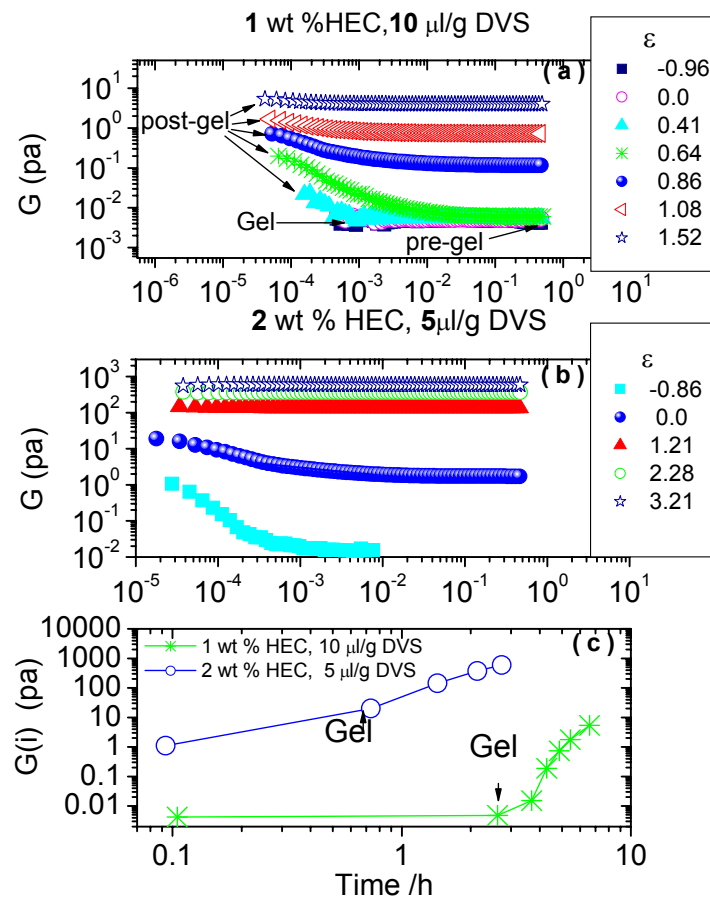


Figure 47. Shear relaxation modulus versus time at different stages of gelation for 1 wt % and 2 wt % HEC solutions at a cross-linker concentration of 10 $\mu\text{l/g}$ and 5 $\mu\text{l/g}$, respectively (every 5th point is shown). Graph (c) shows changes of the initial shear relaxation modulus during the gel evolution.

3. Small Angle Neutron Scattering (SANS)

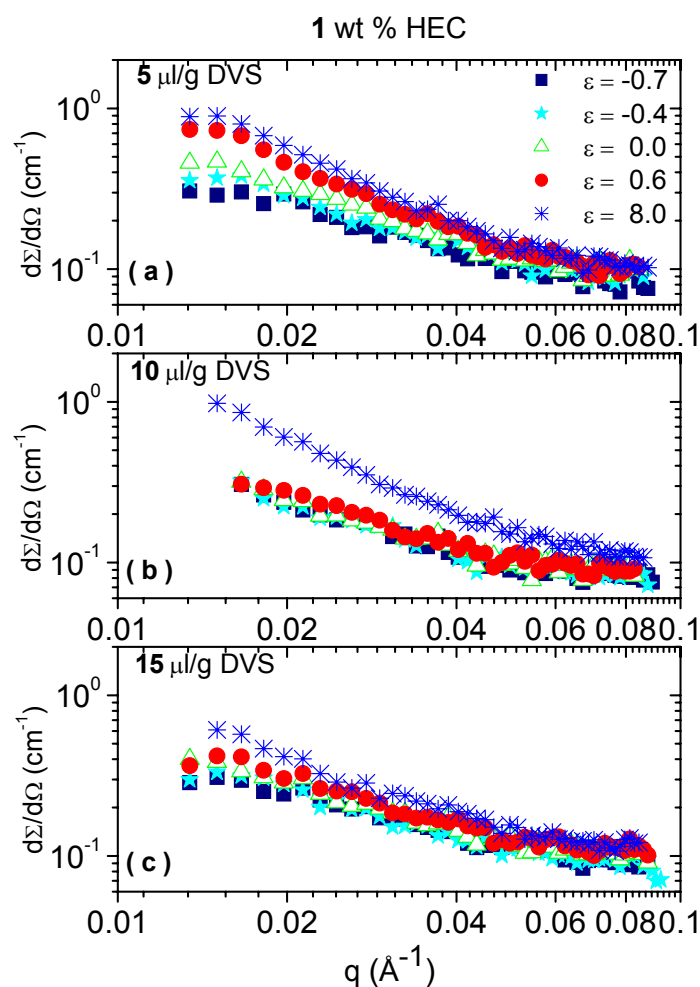


Figure 48. SANS scattered intensity plotted versus the scattering vector q for 1 wt % HEC samples with different cross-linker concentrations at various stages of gelation.

To shed light on the structure of HEC networks on a mesoscopic dimensional scale, SANS measurements on gelling samples with different levels of cross-linker addition, and on gels that have been quenched at a certain stage, have been carried out. The q dependencies of the scattered intensity during the gelation process for a 1 wt % HEC solution with different amounts of DVS are depicted in *Figure 48*. To be able to monitor the gelation process at various stages, and to maintain a sufficiently strong

signal with good statistics from the SANS measurements, it was necessary to limit the considered q range. The intention was to probe possible changes of the network structure in the course of gelation. The general feature that can be traced in the spectra is the stronger upturn of the scattered intensity at low q values for gels that have been cured for a long time. This is again an indication of that the heterogeneities within the gels grow during the curing process.

Figure 49 shows SANS results over a broader q -range for gels with different cross-linker concentrations that have been quenched after a certain time ($\varepsilon \approx 0.4$). A salient feature is the progressively stronger upturn of the scattered intensity at low q values as the level of cross-linker addition is increased. This upturn can be described by a power law, with a slope of approximately -2.1 for the sample with the highest cross-linker concentration. In this q regime the scattered intensity is determined by large-scale fluctuations of the polymer concentration and this feature has been ascribed to the formation of multichain domains.⁷² A higher value (-3.6) of the slope has been observed for charged⁷³ and neutralized⁷⁴ polyacrylate hydrogels. It was argued⁷⁴ that this value reflects the presence of surfaces (an exponent z of 4 suggests a Porod scattering law⁷⁵ from surfaces), and the behavior was attributed to the presence of large frozen-in structural inhomogeneities. The upturn in the scattering profile at low q values has previously been reported^{72,76,77} for polymer systems of various natures and values of the power law exponent z from approximately 2 to 4 have been found. In the light of these observations, the results in the low q regime indicate the existence of large association complexes, which likely originate from cross-link zones.

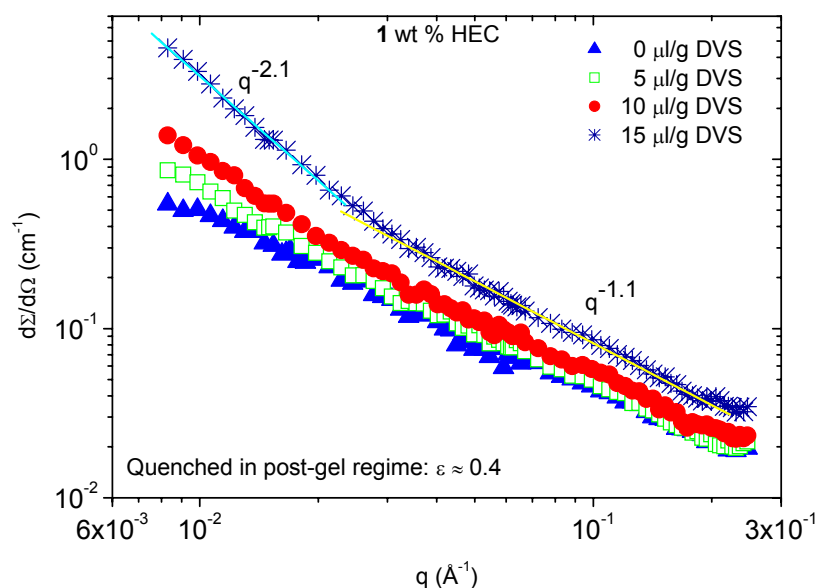


Figure 49. SANS scattered intensity plotted versus the scattering vector q for 1 wt % nongelling and gelled HEC samples with different cross-linker concentrations. For the gels, the cross-linker reaction has been quenched at a certain stage ($\varepsilon \approx 0.4$).

In the higher q -range, all the curves display an intensity that varies approximately as $q^{-1.1}$. This dependency corresponds virtually to the characteristic rod-like behavior of semirigid polymer chains when we look at smaller distances than the persistence length. This suggests that the HEC chains are locally stretched, and it seems that the cross-linker reaction does not affect the local structure of the network. The only visible effect is the higher values of the scattered intensity as the cross-linker concentration is increased. The q^{-1} dependency of the scattered intensity at higher q values has been reported^{64,78} previously from SANS experiments on various polysaccharide systems. In this context, it is interesting to note that a q^{-1} dependency of the scattered intensity was observed from light scattering measurements on a dilute HEC solution with DVS at different stages of quenching (See the discussion above).

4. Dynamic Light Scattering (DLS)

The highest cross-linker concentration (15 $\mu\text{l/g}$), employed in the other experiments, has not been included in the DLS study because the fast gelation of HEC at this DVS level causes alterations of the sample in the course of measurement and this may yield unreliable data.

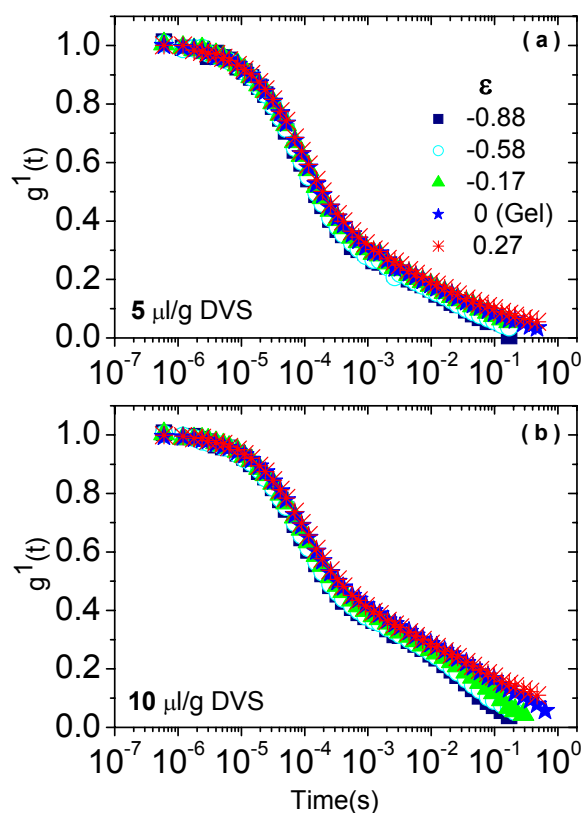


Figure 50. Plot of the first order electric field correlation function as a function of time for 1 wt % HEC with 5 and 10 $\mu\text{l/g}$ DVS.

Figure 50 displays the correlation functions for 1 wt % HEC with 5 and 10 $\mu\text{l/g}$ DVS. The curves are fitted with the aid of eq. 28. The correlation functions can be described by a single exponential, followed by a stretched exponential at longer times. The curves reveal a gradually increase of the slow relaxation times as the cross-linking

proceeds in the solutions. This behavior has been observed before in many other systems in different conditions.^{60,61,79}

Figure 51 shows the normalized time correlation data, together with some curves fitted with the aid of eq. 28, at various stages during the gelation process for a 1 wt % HEC solution at two different levels of cross-linker addition. The general trend at all stages is that the long-time tail of the correlation function is shifted toward longer times as the gel evolves, and this effect is more pronounced at the highest cross-linker concentration. At all conditions, the correlation functions can be well described by means of eq. 27 and the samples exhibit *ergodic* features ($B > 0.6$).

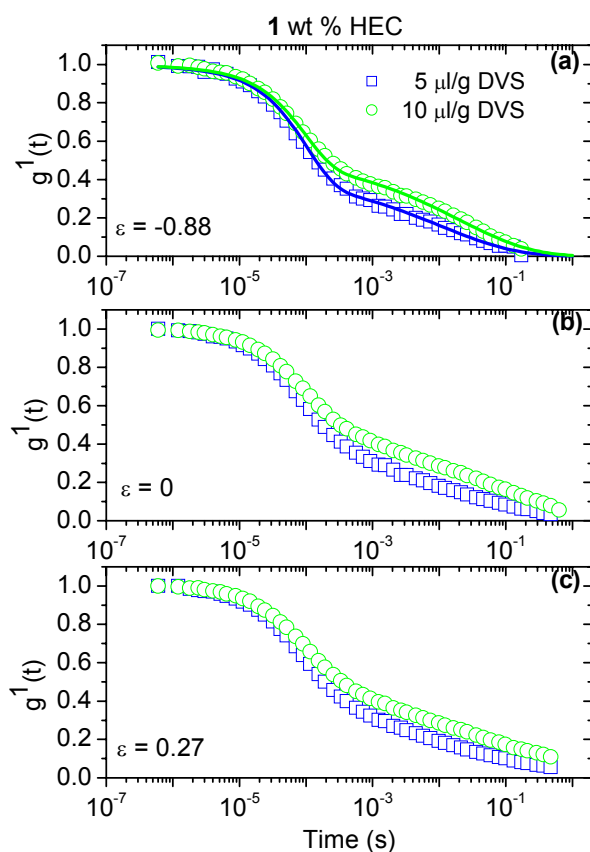


Figure 51. First-order electric field correlation function versus time (every third data point is shown) at a scattering angle of 90° for 1 wt % HEC solutions with two cross-linker concentrations at different stages (ϵ) during the cross-linking reaction.

The variations of the cooperative diffusion coefficient D_c ($\tau_f^{-1} = D_c q^2$), the slow relaxation time τ_s , and the reduced intensity as a function of ε are depicted for the two considered DVS concentrations in *Figure 52*. The value of D_c drops as the gel is formed, and in the post-gel region the decrease of D_c is stronger for the sample with the higher level of cross-linker addition. These features can probably be associated with nonuniformities of the network.³ It has been reported⁸⁰ that nonuniformities in the network structure play an important role for the diffusion properties. This model predicts a reduction of the diffusion coefficient for a gelling system with increasing nonuniformity. In the light of this approach, the present diffusion results suggest that the nonuniformities of the network increase as the gelation process proceeds, and the effect is enhanced as the cross-linker concentration is increased. This is consistent with the overall picture that emerges from this investigation. The influence of cross-linker addition on the slow relaxation time during gelation is illustrated in *Figure 52b*. The results reveal that the slow relaxation process is slowed down as the cross-linking reaction proceeds, and this trend becomes more pronounced with increasing DVS concentration. This is expected because as more and more chains are cross-linked the chain relaxation should be hampered, and longer relaxation times are foreseen. The same results have also been reported for other systems.^{51,57}

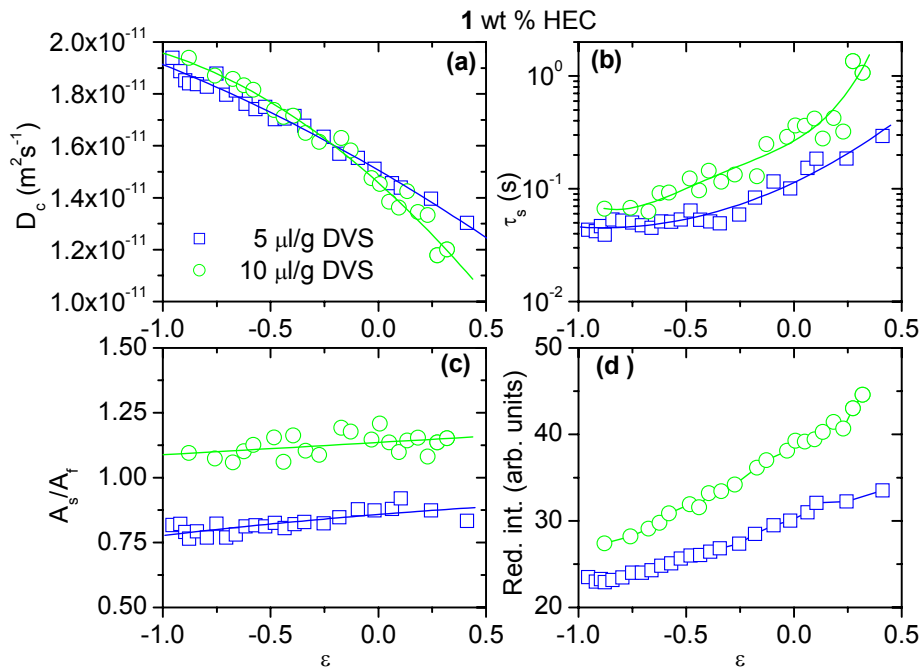


Figure 52. Variations of the cooperative diffusion coefficient (a), the slow relaxation time (b), the ratio A_s/A_f (c), and the reduced intensity (d) as a function of ε for 1 wt % HEC at the cross-linker concentrations indicated.

The results for the ratio A_s/A_f during gelation (*Figure 52c*) show that the contribution from the slow mode increases slightly in the course of gelation and higher values of the ratio are observed at the highest cross-linker density. At both cross-linker concentrations, the value of the stretched exponential β decreases from about 0.4 to 0.3 as the gelation process proceeds, suggesting a broader distribution of relaxation times. These features are probably a result of enhanced structural heterogeneity of the samples and that a connected gel-network is established.

Figure 52d shows the effect of cross-linker density on the reduced scattered intensity during the time evolution of the gel. The results indicate that the large-scale structural inhomogeneities of the samples grow during the gelation process, and this

growth is promoted by increasing cross-linker concentration. The gelation induces large-scale heterogeneities, probably arriving as a result of formation of cross-linker zones. An increase in relaxation time during the gelling process has also been observed for various gelling systems.^{59,82}

VI. Conclusions

In this work, some novel information about the influence of steady shear flows on intramolecular and intermolecular association in *dilute* aqueous solutions of hydroxyethylcellulose in the presence of a cross-linker agent have been reported. Dynamic light scattering results at quiescent conditions reveal no intrachain contraction but only multichain aggregation. The weak perturbation caused by the Brownian dynamics will favor intermolecular association and possible intramolecular association is overshadowed. The growth of the aggregates starts at earlier times when the cross-linker concentration increases. After quenching to a lower pH, the growth of the species is arrested.

At moderate shear rates, the large number of hydroxide groups on the individual chain will come close to each other through rotation of the chains and form intramolecular cross-links. As time goes by, the moieties will collide with each other many times and gradually large aggregates will be buildup via interpolymer cross-linking. The commencement and magnitude of these features depend on factors such as shear rate, polymer concentration, and cross-linker density.

Rheological, dynamical, and structural changes of *semidilute* HEC samples during the chemical gelation of these systems have been examined. The steady shear measurements reveal that the shear rate dependency increases by increasing the polymer concentration. The rheological findings have clearly demonstrated that higher polymer and cross-linker concentrations promote a faster gelation and a stronger incipient hydrogel. Both shear viscosity and relaxation measurements reveal that strong gel-network structures are formed far beyond the gel points.

The general picture that emerges from SANS is that the formation of cross-linker zones during the gelation process gives rise to large-scale heterogeneities in the gels, which grow in intensity as the cross-linker reaction proceeds. The slow relaxation process is slowed down as the gel evolves, because more chains are cross-linked.

The SANS experiments carried out in this study allowed us to access information concerning the structural organization of hydrogels in terms of concentration fluctuations on mesoscopic length scales. In the low q -range, an upturn in the scattered intensity is detected and this effect becomes more pronounced as the cross-linker concentration in the gel is increased, due to the growth of the heterogeneities in the gel by increasing the cross-linker concentration. In the high q -range, no effect of cross-linker concentration on the morphology can be detected on this short length scale. The q dependency of the scattered intensity in this regime signals that the polymer chains are locally stretched. This work has shown that by changing the cross-linker density and the curing time, the mechanical and structural features of the hydrogel can be tuned for certain applications in e.g., pharmaceutical formulations.

VII. Appendix

Table 3 shows some characteristic results for HEC samples.

Table 3. Some Results from Different Techniques

Some Characteristics of HEC	C^* : 0.25 wt %	$C^* = 1/[\eta]$			See page 52
	CP : 100°C	Ref. 22			
	$M_w \approx 400,000$	By the aid of Zimm-plot			
	$A_2 : 7.41E-4$	By the aid of Zimm-plot/ Showing a good thermodynamic condition ($A_2 = 0 \rightarrow \theta$ Condition)			
	$R_g : 1089 \text{ \AA}$	By the aid of Zimm-plot			
Semidilute HEC					
1 wt % HEC	5 $\mu\text{l/g}$ DVS	10 $\mu\text{l/g}$ DVS	15 $\mu\text{l/g}$ DVS		
GP	221 min	157 min	129 min	See Page 34	
m	-0.28	-0.37	-0.38	See Page 34	
n	0.72	0.67	0.67	See Page 35	
S	0.08	0.13	0.19	See Page 35	
2 wt % HEC	5 $\mu\text{l/g}$ DVS	<ul style="list-style-type: none"> ❖ The polymer concentration plays an important role for the dynamical structure of the network. ❖ GP decreases with increasing HEC and DVS concentrations. ❖ Higher S and lower m lower values of m suggest a stronger network. ❖ Lower value of n reveals a higher aggregation and entanglements in the solution. 			
GP	39 min				
m	-0.46				
n	0.54				
S	1.05				

VIII. References

1. Kjøniksen, A.-L.; Knudsen, K. D.; Nyström, B. *European Polymer Journal* **2005**, 41, 1954.
2. Walderhaug, H.; Kjøniksen, A.-L.; Nyström, B. *Journal of Physical Chemistry B* **1997**, 101, 8892.
3. Kjøniksen, A.-L.; Nyström, B. *Macromolecules* **1996**, 29, 5215.
4. Bu, H.; Kjøniksen, A.-L.; Knudsen, K. D.; Nyström, B. *Biomacromolecules* **2004**, 5, 1470.
5. McConville, P. and Pope, J. M., *Polymer* **2000**, 41, 9081.
6. Lloyd, L. L.; Kennedy, J. F.; Methacanon, P.; Paterson, M. and Knill, C. J. *Carbohydrate Polymers* **1998**, 37, 315.
7. Šimkovic, I.; Hricovini, M. and Sasinková, V. *Carbohydrate Polymers* **2002**, 47, 131.
8. Reboiras, M. D. *Journal of Membrane Science* **1994**, 92(1), 75-84.
9. Wiley, J. and Sons, *Encyclopedia of Polymer Science and Engineering*, **1987**, 7.
10. Nyström, B. ;Kjøniksen, A.-L. ; Iversen, C. *Advanced Colloid Interface Science* **1999**, 79, 81.
11. Aamer, K. A. ; Sardinha, H. ; Bhatia, S. R. ; Tew, G. N. *Biomaterials* **2004**, 25, 1087.
12. Kjøniksen, A.-L. ; Nyström, B. ; Lindman, B. *Macromolecules* **1998**, 31, 1852.
13. Gilsenan, P. M.; Richardson, R. K.; Morris, E. R. *Carbohydrated Polymer* **2000**, 41, 339.
14. Barbier, V. ; Hervé, M.; Sudor, J.; Brulet, A.; Hourdet, D.; Viovy, J.-L. *Macromolecules* **2004**, 37, 5682.
15. Sannino, A.; Madaghiele, M.; Conversano, F.; Mele, G.; Maffezzoli, A.; Netti, P. A.; Ambrosio, L.; Nicolais, L. *Biomacromolecules* **2004**, 5, 92.
16. Boyko, V.; Richter, S. *Macromolecular Chemistry and Physics* **2004**, 205, 724.

17. Omari, A.; Chauveteau, G.; Tabary, R. *Colloids and Surfaces, A: Physicochemical and Engineering Aspects* **2003**, 225, 37.
18. Lu, X.; Hu, Z.; Gao, J. *Macromolecules* **2000**, 33, 8698.
19. Murry, M. J.; Snowden, M. J. *Advanced in Colloid and Interface Science* **1995**, 54, 73.
20. Wiley, J. and Sons, *Encyclopedia of Polymer Science and Engineering*, **1989**, 17.
21. Wiley, J. and Sons, *Encyclopedia of Polymer Science and Engineering*, **1985**, 3.
22. Nilsson, S. Ph.D. thesis, *Lund University*, Center for Chemistry and Chemical Engineering **1999**.
23. Liu, S.; Weaver, J. V. M.; Save, M. and Armes, S. P. *Langmuir* **2002**, 18, 8350.
24. Schmitz, K. S.; Wang, B.; Kokufuta, E. *Macromolecules*, **2001**, 34, 8370.
25. Lipatov, Y. S. *Colloid Chemistry of Polymers* **1988**, Academy of Sciences of the Ukranian SSR.373.
26. Rubinstein, M.; Colby, R. H. *Macromolecules* **1994**, 27, 3184.
27. Tanaka, F.; *Macromolecules* **1994**, 27, 3943.
28. Wiley, J. and Sons, *Encyclopedia of Polymer Science and Engineering*, **1989**, Supplement volume.
29. Wiley, J. and Sons, *Encyclopedia of Polymer Science and Engineering*, **1988**, 14.
30. Ronald G., L. *The Structure and Rheology of Complex Fluids* **1999**, University of Michigan.
31. Goodwin, J.W. and Hughes, R.W. *Rheology for Chemists-an introduction* **2000**, Cambridge: The Royal Society of Chemistry.107-112.
32. Winter, H. H.; Chambon, F. *Journal of Rheology* **1986**, 30, 367.
33. Scanlan, J. C.; Winter, H. H. *Macromolecules* **1991**, 24, 47.
34. Winter, H. H. *Progress in Colloid and Polymer Science* **1987**, 75, 104.

35. Martin, J.E.; Adolf, D.; Wilcoxon, J. P. *physical Review Letters* **1988**, 61, 2620;
Phys.Rev. A **1989**, 39, 1325.
36. Martin, J. E.; Adolf, D. *Annual Review of Physical Chemistry* **1991**, 42, 311.
37. De Gennes, P.-G. *Scaling concepts in polymer physics*; Cornell University Press:
Ithaca, NY, 1979.
38. Alexander, S. *Journal of Physics (Paris)* **1984**, 45, 1939.
39. Muthukumar, M. *Journal of Chemical Physics* **1985**, 83, 3161.
40. Cates, M. E. *Journal of Physics (Paris)* **1985**, 46, 1059.
41. Muthukumar, M. *Macromolecules* **1989**, 22, 4656.
42. Schiessel, H.; Blumen, A. *Macromolecules* **1995**, 28, 4013.
43. Groot, R. D.; Agterof, W. G. M. *Macromolecules* **1995**, 28, 6284.
44. Winter, H. H. In *Encyclopedia of Polymer Science and Engineering. Supplement*
Volume; Wiley: New York, **1989**; 343
45. Wiley, J. and Sons, Edited by Avnir, D.; *The Fractal Approach to Heterogeneous*
Chemistry **1989**, 68.
46. Kjøniksen, A.-L.; Laukkanen, A.; Galant, C.; Knudsen, K. D.; Tenhu, H. and
Nyström, B. *Macromolecules* **2005**, 38, 948.
47. Galant, C.; Kjøniksen, A.-L.; Knudsen, K. D.; Helgesen, G.; Lund, R.; Laukkanen, A.;
Tenhu, H. and Nyström, B. *Langmuir* **2005**, 21, 8010.
48. Knudsen, K. D.; Fossum, J. O.; Helgesen, G.; Haakestad, M. W.; *Physica B* **2004**,
352, 247.
49. Bale, H. D.; Schmidt, P.W. *Physical Review Letters* **1984**, 53, 596.
50. Harding, S.E.; Sattelle, D.B.; Bloomfield V.A., *Laser Light Scattering in Biochemistry*
1992, Cambridge: The Royal Society of Chemistry
51. Kjøniksen, A.-L. and Nyström, B. *Macromolecules* **1996**, 29, 7116.

52. Min, G.; Savin, D.; Gu, Z.; Gu, Patterson, G. D.; Kim, S. H.; Ramsay, D. J.; Fishman, D.; Ivanov, I.; Shenja, E.; Slaby, E.; Oliver, J. *International Journal of Polymer Analysis and Characterization* **2003**, 8, 187.
53. Bhatia, S.; Barker, J.; Mourchid, A. *Langmuir* **2003**, 19, 532.
54. Bhatt, M.; Jamieson, A. M. *Macromolecules* **1988**, 21, 3015.
55. Siegert, A. J. F. *Massachusetts Institute of Technology* **1943**, Radiation Laboratory, Report No. 465.
56. Ngai, *Advanced Colloid Interface Science* **1996**, 64, 1.
57. Nyström, B. and Walderhaug, H. *Journal of Physical Chemistry* **1996**, 100, 5433.
58. Fang, L.; Brown, W. *Macromolecules* **1990**, 23, 3284.
59. Nyström, B.; Lindman, B. *Macromolecules* **1995**, 28, 967.
60. Nyström, B.; Walderhaug, H.; Hansen, F. K. *Journal of Physical Chemistry* **1993**, 97, 7743.
61. Sun, Z.; Wang, C. H. *Macromolecules* **1994**, 27, 5667.
62. Torres, F. E.; Russel, W. B.; Schowalter, W. R. *Journal of Colloid and Interface Science* **1991**, 142, 554.
63. Martin, J.; Wilcoxon, J. P. *physical Review Letters* **1988**, 61, 373.
64. Buhler, E.; Boué, *Macromolecules* **2004**, 37, 1600.
65. Maleki, A.; Beheshti, N.; Kjøniksen, A.-L. and Nyström, Bo. Shrinking of Chemically Cross-Linked Polymer Networks in the Postgel Region, *in preparation*.
66. Nyström, B.; Walderhaug, H.; Hansen F. K. *Langmuir* **1995**, 11, 750.
67. Nakken, T.; Tande, M.; Nyström, B. *European Polymer Journal* **2004**, 40, 181.
68. Cox, W. P.; Merz, E. H. *Journal of Polymer Science* **1958**, 28, 619.
69. Baldursdóttir, S. G.; Kjøniksen, A.-L.; Karlsen, J.; Nyström, B.; Roots, J. and Tønnesen, H. H. *Biomecromolecules* **2003**, 4, 429.

70. Winter, H. H. and Mours, M. *Advances in Polymer Science* **1997**, 134, 166.
71. Koike, A.; Nemoto, N.; Takahashi, M.; Osaki, K. *Polymer* **1994**, 35, 3005.
72. Ermi, B. D.; Amis, E. J. *Macromolecules* **1997**, 30, 6937.
73. Horkay, F.; Bassler, P. J. Hecht, A.-M.; Geissler, E. *Polymer Preprints* **2002**, 43, 360.
74. Horkay, F. Hecht, A.-M. Grillo, I; Bassler, P. J.; Geissler, E. *Journal Chemical Physics* **2002**, 117, 9103.
75. Glatter, O.; Kratky, O. *Small angle X-ray Scattering*, Academic Press: London, **1982**.
76. Shibayama, M.; Tanaka, T. *Journal of Chemical Physics* **1995**, 102, 1995.
77. Wesley, R. D.; Cosgrove, T.; Thompson, L.; Armes, S. P.; Baines, F. L. *Langmuir* **2002**, 18, 5704.
78. Esquenet, C.; Terech, P.; Boué, F.; Buhler, E. *Langmuir* **2004**, 20, 3583.
79. Nyström, B.; Thuresson, K.; Lindman, B. *Langmuir* **1995**, 11, 1994.
80. King, S. M. *Large-Scale Structure Group*, **1995**, ISIS Facility.
81. Horkay, F.; Burchard, W.; Geissler, E.; Hecht, A.-M. *Macromolecules* **1993**, 26, 1296.